FUNCTIONAL VALIDATION OF A NOVEL TECHNIQUE FOR ASSEMBLING HIGH DENSITY POLYIMIDE COCHLEAR IMPLANTS

A Thesis
Presented to
The Academic Faculty

By

Alton Russell Sharpe

In Partial Fulfillment
Of the Requirements for the Degree
Master of Science in BioEngineering

Georgia Institute of Technology

December, 2012

FUNCTIONAL VALIDATION OF A NOVEL TECHNIQUE FOR ASSEMBLING HIGH DENSITY POLYIMIDE COCHLEAR IMPLANTS

Approved by:

Dr. Pamela T. Bhatti, Advisor
School of Electrical and Computer Engineering
Georgia Institute of Technology

Dr. Robert J. Butera
School of Electrical and Computer Engineering
Georgia Institute of Technology

Dr. Thomas J. Burkholder
School of Applied Physiology
Georgia Institute of Technology

Date Approved: March 12, 2012

ACKNOWLEDGEMENTS

Funding for this work was provided in part by the National Science Foundation, grant CBET-1133625. The Insertion Platforms were provided in kind by MED-EL Corporation (Innsbruck, Austria).

Special thanks go to the members of the thesis reading committee for their guidance in presenting this work. The contributions of Dr. Brian J. McKinnon and Dr. Jessica Van Beek-King of the Georgia State Health University as well as the Georgia Institute of Technology Machine shop are also acknowledged for being instrumental to the successful completion of this Master's thesis.

TABLE OF CONTENTS

LIST OF TABLES

LIST OF FIGURES

SUMMARY

This work begins with an introduction to the physiology of hearing loss including its proposed mechanisms and the impacts of noise trauma. The review will conclude by briefly discussing the capabilities of current hearing aid solutions and the point at which they are no longer beneficial, necessitating a device capable of directly stimulating the peripheral auditory nerves – the cochlear implant. Cochlear Implant technology will then be discussed and will focus on techniques for improving frequency resolution, ultimately introducing our work with Thin-Film Array technology to increase electrode site density.

The experimental work overview involves a detailed description of a novel assembly process for combining the thin film arrays with structural backings required for surgical insertion, and will specifically highlight the steps taken to avoid issues that arose in the previous generation of assemblies. The motivation for selective flexibility of the array in certain planes will be introduced, and the desire for a pre-curved array to influence both thin-film array adhesion and electrode flexibility will be discussed. Finally, the new assembly process is validated mechanically through finite-element simulation in COMSOL, physical deflection force characterization, and a surgical insertion study. Impedance testing of the active sites will attempt to evaluate any effects that the above processes have on the electrical performance of the electrode assemblies. It is shown that the new assembly procedure is able to create a selectively flexible array that reduces shearing strains between the thin-film arrays and surgical backings, resulting in assembled electrode arrays that may lead to reduced insertion trauma.

CHAPTER 1: INTRODUCTION

Hearing loss is a physical disability that affects over 37 million adults in the United States alone, making it the most prevalent of any major disability [1]. Of these individuals, approximately 71,000 have received cochlear implants due to the severity of their hearing loss [2]. Candidacy for becoming a cochlear implant recipient requires an individual to have profound hearing loss approaching deafness such that there is no benefit from a traditional hearing aid. At this point the natural signal transduction pathway of converting mechanical vibrations of acoustic events into neural impulses is almost completely non-functional. While this can sometimes be the result of bone conduction malfunctions in the middle ear, the majority of hearing loss is sensorineural related: the inner ear transduction mechanisms do not effectively generate neural impulses. However, the auditory nerves often remain intact and highly functional, meaning that some method of directly stimulating them could lead to a restoration of some degree of natural hearing.

Cochlear implants were developed specifically for this purpose. In 1957 the first device for stimulating the auditory nerve was implanted [3], and further developments ultimately led to a pivotal 1972 feasibility study by the NIH to determine the potential of full-fledged support of cochlear implant development [4]. This report positively concluded that the implant technology to date successfully helped recipients score higher on speech recognition tests, leading to the creation and funding of the Neural Prosthesis Program. Implant and speech processor technology has been improving rapidly since that point and has partly focused on increasing the number of active electrodes, but has always been constrained by the conventional technology used for implants: silicone based wire-core electrodes. The diameter of the scala tympani in the human cochlea, where an implant is typically placed, on average tapers from 2 mm at the basal end to 200 um at the apex [5]. Therefore, the anatomy of the canal places an upper bound on

the total width of the electrode, which is directly proportional to the number of wires leading to the active sites that can be bundled together. Modern day commercially available arrays have between 12 and 22 electrodes, and while this number of electrodes often leads to acceptable scores for patients on speech recognition tests [3] it follows intuitively that a discrete system such as this which intends to represent an effectively continuous natural structure would benefit from an increase in the discrete “resolution” of the system.

To this end, we continue previous work [6, 7] on a novel approach to cochlear implant electrodes based upon flexible polyimide Thin-Film Array (TFA) technology. These arrays are made with standard MEMS fabrication techniques and contain platinum electrode sites in a much higher density than anything commercially available. However, these arrays are too thin and flexible to be effectively inserted into the cochlea and require some means of surgical backing to provide the necessary structural rigidity to attain an adequate insertion depth. Previous work attempting to bond the arrays to surgical Insertion Test Devices (ITDs) provided by MED-EL (MED-EL Corporation, Innsbruck, Austria) [8] showed promise but revealed significant difficulties in maintaining adhesion between the array and ITD throughout surgical insertion. In order to combat these issues, new adhesion procedures will be developed and a machined mold will be used to promote structurally sound adhesion of the two units. Use of less rigid Insertion Electrodes (IEs) as surgical backings will also be explored.

Final validation of the assembled electrodes will be done both structurally and electrically. Finite-element modeling of full assemblies as well as the components used will theoretically quantify the manner in which the assemblies deform due to tip forces, and these results will then be compared with a physical test of deflection forces. An insertion study on human cadaver cochleae will determine how effectively the assemblies withstand standard surgical implantation techniques, and electrical impedance testing will determine how the electrode’s performance is affected by the mechanical assembly and insertion procedures.

CHAPTER 2: THE PHYSIOLOGY OF HEARING LOSS

2.1 Overview of the Auditory Pathway

In order to create devices that enhance the human body's ability to transduce sounds we must first understand how it functions normally. The following provides a brief overview of the various physiological components of the auditory system, outlined in Fig. 2.1 below.

2.1.1 The Outer Ear

The auditory pathway begins with the outer ear's visible pinna and subsurface auditory canal and tympanic membrane, or eardrum. For the purposes of this report it is important to consider that the physical shape of the pinna and auditory canal lead to a certain degree of frequency tuning in the outer ear, as well as provide an average of 12 dB of gain to incident sounds. [9] Trauma to the pinna and natural buildup of wax in the ear canal can both lead to a degradation of this natural gain.

2.1.2 The Middle Ear

The middle ear consists of the mallus, incus, and stapes bones which lie in the tympanic cavity and connect the tympanic membrane to the oval window of the cochlea. Vibration of the tympanic membrane is amplified through the lever action of these bones in a ratio of 22:1 as it is delivered to the round window. Patients with hearing loss are often tested for deficiencies in middle ear functionality with a bone conduction test. A vibrating tuning for is placed on the mastoid bone behind the pinna, thus forcing the middle ear bones to vibrate. The patient then compares the perceived loudness of this input with control sound tests. The mechanical

amplification process of the outer and middle ears combined was shown to lead to a pressure increase of up to 18 dB in one study[10].

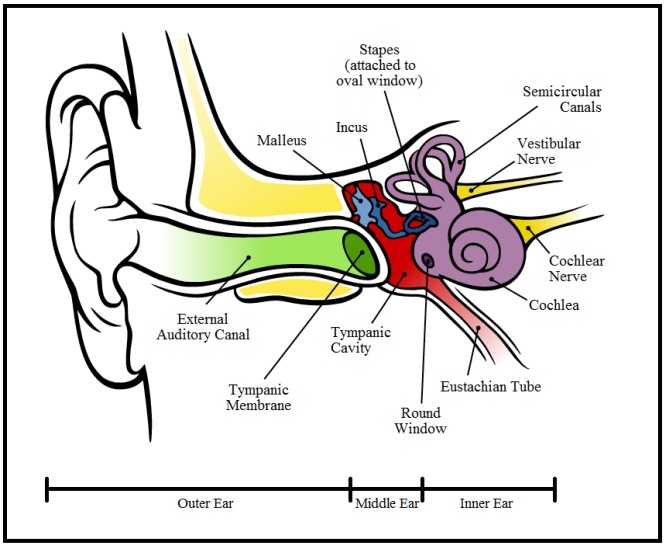

Fig. 2.1 Human ear showing divisions in outer, middle, and inner ear systems. The ear canal length is exaggerated for viewing purposes. [4]

2.1.3 The Inner Ear

The inner ear, consisting of the cochlear and vestibular systems and pictured in Fig. 2.2, is a labyrinth of fluid filled bone. The signal transduction properties of the cochlea are central to this work as it is the place where mechanical vibrations of sound are selectively amplified and converted into electrical impulses.

Vibrations incident to the oval window are converted to fluid vibration of the perilymph contained in the scala tympani and scala vestibuli (see Fig. 2.2). A single pressure wave travels from the oval window at the base of the cochlea up the scala vestibule to the apex where there is an opening to the scala tympani. At this point the wave then travels back down the cochlea through the perilymph of the scala tympani until it reaches the round window back at the base of the cochlea. This up-and-back movement creates a deflection of the basilar membrane, and for a sustained input creates a standing wave on the membrane at a point where its resonance matches the frequency of the input auditory stimulus. At the point of resonance, the deflection of

the basilar membrane causes hair cells of the Organ of Corti to move relative to the tectorial membrane. This movement causes the cilia atop the hair cells, which are physically connected to the tectorial membrane, to bend, opening ion channels in the hair cells and leading to depolarizations and action potentials. Regarding the hair cells, it is important to be aware of the different functions of the inner and outer cells with regard to auditory signal transduction. The outer hair cells are arranged in three rows as shown in image B of Fig. 2.2. These cells are currently believed to contribute to the mechanical amplification and resonance properties of the basilar membrane, although the mechanisms are not entirely understood [11, 12]. The inner hair cells are responsible for innervating the afferent nerves of the auditory peripheral nervous

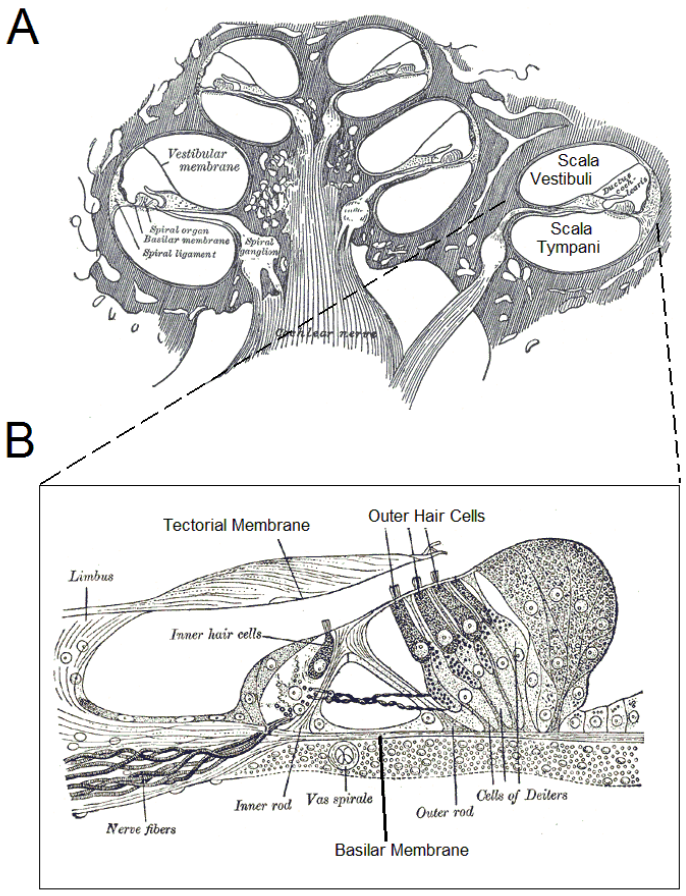

Fig. 2.2 A - Cross-section of the cochlear canals, showing the upper scala vestibuli and lower scala tympani. B - Detailed view of the Organ of Corti, the sensory transduction element of the cochlea. [64]

system.

2.2 Mechanisms of Hearing Loss

Sensorineural hearing loss is the term given to hearing deficiencies that arise from malfunctions of the inner ear or auditory peripheral nervous system. The most common type of sensorineural loss is a result of damage to the outer hair cells due to a combination of genetic and environmental factors such as noise trauma, termed noise-induced hearing loss (NIHL).

As stated previously, outer hair cells play an important role in the amplification and frequency tuning properties of the organ of corti. The outer hair cells were first investigated for these properties for two main reasons. The first is that 95% of afferent nerve endings go to the inner hair cells [13], meaning that outer hair cells play an extremely limited if any role in directly coding audio signals and sending them to the auditory cortex. The second is that passive mechanical models of the cochlea simply do not match physical observations of its performance. Attempted models required excessive damping factors, and even then a manipulation of the model parameters leading to a “good fit” at one end of the cochlea would fall out of line at the other end. [14] Due to these results, models were created that incorporate active mechanical processes in the outer hair cells that feed energy back into the travelling wave. One explanation of the mechanism behind this is that initial depolarization of the outer hair due to basilar membrane deflection causes conformational changes in voltage-dependent motor proteins. These motor proteins contract and expand, leading to changes in cell body length that add to the deflection of the basilar membrane and create positive feedback that leads to the observed sharp tuning properties of the membrane. [13]

Several experiments have been conducted to test the validity of the outer hair cells’ influence on tuning and amplification. One procedure involves electrically stimulating the medial olivocochlear bundle, an efferent neural pathway that ends specifically on the outer hair cells. Hyperpolarization of these nerves leads to a decrease in the mechanical vibration of the basilar

membrane, most noticeably at the point of sharp tuning. [15] A second procedure directly targeted outer hair cells with the cytotoxic drug kanamycin and lead to a broadening of the cochlear tuning ability as well as a 60 dB increase in the threshold of the tuning region. [16] These results clearly show that the outer hair cells play an active role in the tuning and amplification abilities of the cochlear processes, and furthermore that manipulation of their functionality can lead to a decrease in basilar membrane amplitude. Finally, it is important to note that the active properties of the outer hair cells are limited to low intensity stimuli up to about 30 dB SPL, after which point the hair cell response saturates.

2.3 Noise Trauma

Noise Trauma, and specifically impact noise, has been directly linked to loss of functionality and death in outer hair cells. Prolonged exposure to high sound pressure levels understandably leads to mechanical damage of the organ of corti. This includes tearing of hair

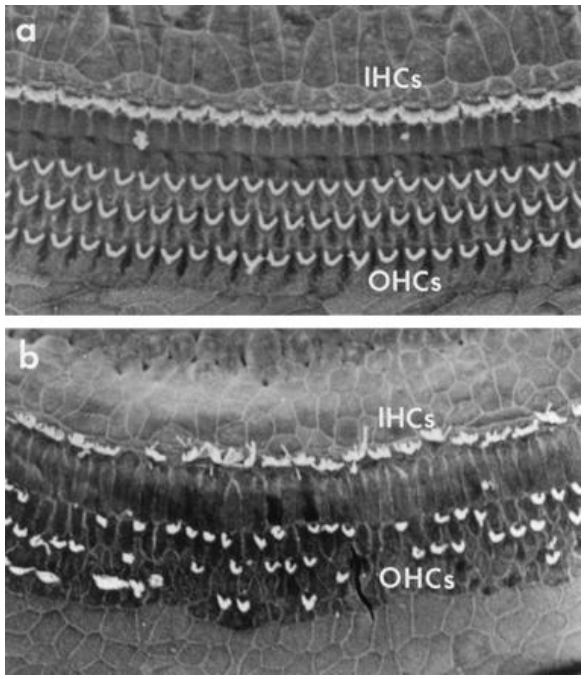

Fig. 2.3 Scanning electron micrographs of the normal (*a*) and damaged (*b*) cochlear sensory epithelium. In the normal cochlea, the stereocilia of a single row of inner hair cells and three rows of outer hair cells are present in an orderly array. In the damaged cochlea, hair cells are missing, and stereocilia are abnormal, leading to hearing loss [19]

cell stereocilia tip-links and rupturing of cell bodies, and at 137 dB shearing of the organ of corti from the bony labyrinth occurs. [17] Impact noise does not involve such high continuous pressures, but instead results in sharper vibrations of the basilar membrane. The active nature of the outer hair cells requires them to expand and contract rapidly, leading to extreme oxidative stress in the cellular environment. Impact noise results in the excessive release of reactive free radical species created through the metabolism of oxygen to fuel the motor proteins' activity. Although free radicals are a natural by-product of cellular metabolic processes, in the event of overwork due to impact noise ithey accumulate faster than the cell can remove them. These molecules lead to DNA breakdowns and damage cellular proteins and lipid membranes to the point where the cell's apoptosis pathway is triggered. [18] The excess of free radicals can lead to temporary and permanent threshold shifts lasting hours or days.

As a side note, it is apparent that protection of the outer hair cells is of key importance when considering methods to guard against noise trauma. Without functioning outer hair cells, as shown in Fig. 2.3, the cochlea loses its ability to amplify low power signals in the 0 to 30 dB range, effectively raising the absolute threshold for sound detection. If noise trauma "overworks" the outer hair cells, then preventative measures should seek to limit the basilar membrane deflection and ultimately the metabolic processes of the outer hair cells that occur during impact noise. A great deal of research has investigated the potential of chemical therapies as preventative and rehabilitative measures. Increased levels of antioxidants will combat the generation of free radicals, and M. Duan et al showed that the antioxidant N-L-acetylcysteine protected the cochlea from threshold shifts during exposure to impulse noise trauma. [20] However, as this study highlighted, the effectiveness of this and similar measures is highly dependent on the dose schedule and the actual concentration of the drug that reaches the ear. Furthermore, outer hair cell loss frequently occurs in individuals who are not exposed to excessive amounts of noise trauma. Advances in human genome sequencing have enabled researchers to identify multiple genes that influence the long-term performance of the auditory

system [62]. In the event that outer hair cell loss does occur and cause hearing impairment, some form of a hearing aid is required to either amplify sounds to a detectable level or directly stimulate the auditory nerves.

2.4 Hearing Aid Solutions

The tendency for our natural hearing capability to degrade over time due to genetic, environmental, or simple aging factors has created the need to develop devices to combat this phenomenon. Of the 37 million Americans who report some degree of hearing loss, those in the range of moderate to severe (50 – 90 dB) loss would benefit from a hearing aid. Traditional hearing aids involve some form of a microphone, amplification system, and speaker that detect incident sounds and amplify them before they hit the tympanic membrane. This ultimately leads to larger displacements of the basilar membrane, enabling recipients to hear sounds that they would not normally have been able to detect. More advanced hearing aids also include degrees of digital signal processing to condition sounds before they are amplified for the purpose of performing tasks such as dynamic range compression and vocal isolation in noisy environments.

As effective as hearing aids can be for this category of individuals, it has a prerequisite of some degree of residual hearing. This means that a certain number of functional hair cells must still be present in the cochlea in order to translate mechanical vibrations into neural impulses. For individuals that have profound hearing loss or are completely deaf, effectively no amount of mechanical sound amplification will lead to a useable sensation of hearing. This is the underlying problem which a cochlear implant serves to address: to bypass the function of the hair cells entirely and deliver the sensation of hearing by directly stimulating the peripheral auditory nerves.

CHAPTER 3: THE COCHLEAR IMPLANT

The previous section introduced the concept of a cochlear implant, a device that directly stimulates the auditory nerves of the inner ear. This chapter provides a brief overview of the history of implant development and includes a physical description of current technologies. An important concept to consider is the signal processing methodology that is applied to incident sounds to deliver the most effective electrical stimulation patterns to peripheral auditory nerves to recreate the perception of sound. Also, limitations of current technology will be discussed in order to introduce the motivation for this work on next-generation technology.

3.1 History of the Cochlear Implant

The first cochlear implantation was performed in 1957 and consisted of a rudimentary inductance coil that terminated on the stump of the auditory brainstem [3]. The patient was able to detect the presence of environmental sound but could not distinguish tones or speech due to the nature of the device. This was essentially a proof-of-concept that showed that electrical stimulation of auditory nerves could be translated into some perception of sound, and the need for a higher resolution system motivated the use of multiple electrodes for multiple channels of stimulation. This enabled devices to selectively stimulate at different frequencies, thus providing a more accurate representation of natural sound. An NIH conference in 1988 concluded that multi-channel stimulation was able to restore a patient's hearing to the point where they could carry on normal conversations without lip-reading [21]. Improvements in implant design and processing techniques continued, and by 1995 a second NIH consensus concluded that a majority of cochlear implant recipients could score above 80% correct on speech comprehension tests [22]. Since this time there have not been drastic changes to implant

technology, and a majority of developments have focused on refinements in speech processing algorithms.

3.2 Anatomy of an Implant

3.2.1 Overview

A modern cochlear implant is made up of three major components: an external, behind-the-ear microphone and DSP speech processor; an inductive transcutaneous link to an implanted receiver coil; and a silicone based wire-core electrode implanted into the cochlea. Fig. 3.1 shows an overview of these components and their placement upon implantation of a device. The behind-the-ear unit, labeled (1), is very similar to a traditional behind-the-ear hearing aid in both form-factor and purpose. Its omni-directional microphones pick up ambient sounds which it

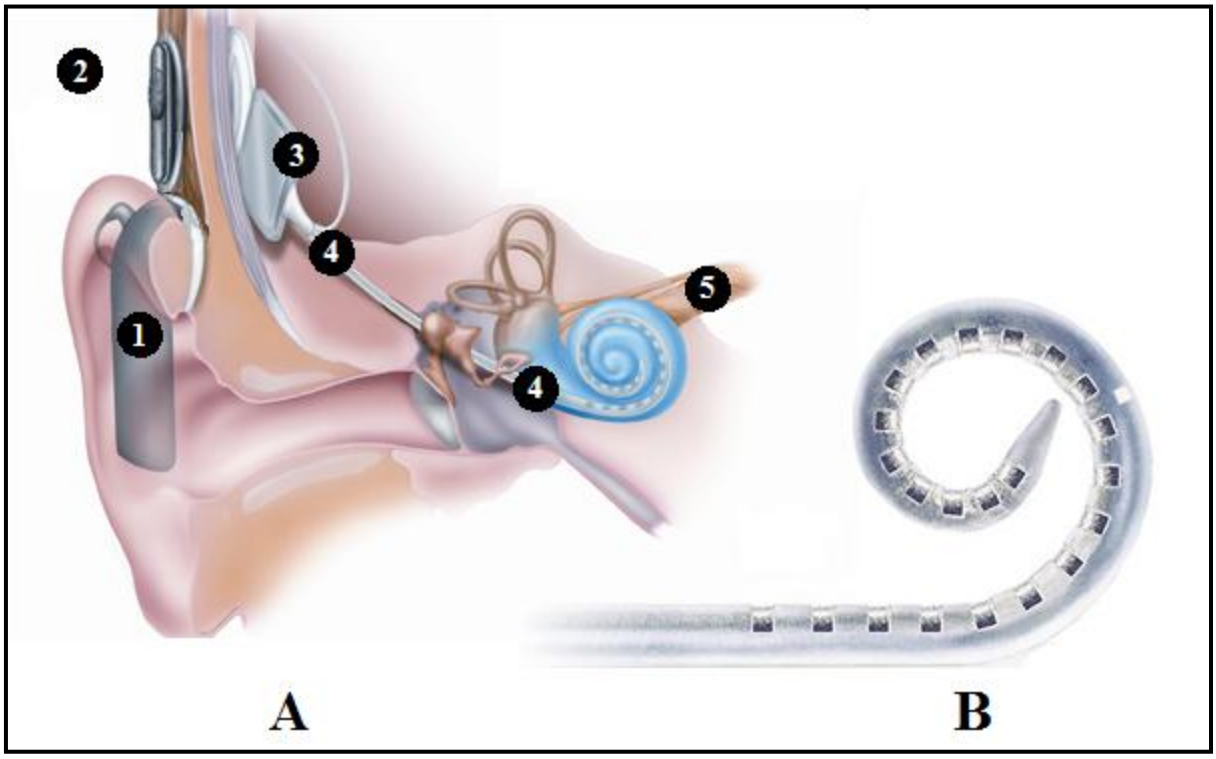

Fig. 3.1 A: Overview of the major components of a cochlear implant as they are positioned after implantation. (1) Microphone, DSP circuitry, and battery worn behind the ear, (2) External RF Transmitter, (3) Subcutaneous RF receiver and stimulator hardware, (4) Electrode Array, (5) Peripheral auditory nerve bundle. B: Enlarged view of a traditional silicone-based wire core electrode array [23]

then digitizes in order to condition them through various stages of digital signal processing. However, this is where functionality diverges from a standard hearing aid. The signal processing that occurs alters the audio in significantly different ways in order to most effectively create electrical impulses, which will be discussed in the following sections. A short external wire runs from the processor to the External RF transmitter (2). This inductive coil is held in place by magnetic attraction to the Implanted RF receiver (3), and together these units allow wireless transmission of high energy signals to the implanted hardware. This wireless transmission of energy means that the implanted portion of the device needs no internal power source and, from an operational standpoint, does not ever need to be accessed after the initial implantation procedure unless there is some type of malfunction. The implanted receiver includes decoding circuitry to transform the conditioned signal into pulses that are then sent to the electrodes at the end of the electrode array (4) inserted into the cochlea. The array is typically inserted through a cochleostomy hole or the round window of the cochlea (refer back to Fig. 2.1) where there is a flexible membrane that seals off the scala tympani, and it is usually inserted to a depth of 22-30 mm [24]. Effective electrical depolarization of nerve cells along the cochlea leads to transmission of neural impulses along the vestibulocochlear (8^{th} Cranial) nerve (5) and into the auditory cortex of the central nervous system.

3.2.2 Ideal Electrical and Mechanical Properties of Electrode Arrays

The electrode array form factor and composition are of specific importance to this research work, and its electromechanical properties determine its functional and physical performance. Fig. 3.1 B provides a good example of a conventional silicone based wire-core electrode array. Arrays of this nature tend to be limited in the number of electrodes that they can contain because every electrode requires a lead wire, contained in the silicone, to run back to the implanted receiver. The summed diameter of the lead wires accumulates as more electrodes are added, and at a certain point there is no more room for additions while still being

able to fit safely within the narrow confinements of the scala tympani. According to M. Zrunek et al., the human scala tympani ranges in dimension from 1.25 x 1.66 mm (height x width) at the opening of the round window to .78 x 1.3 mm at 450 degrees of insertion, which is a standard maximum depth of array insertion [25]. Taking the height as a limiting factor, it follows that commercially available electrode arrays range in diameter from 1.1 to .6 mm [7].

Mechanically, and ideal electrode array will allow for perimodiolar placement within the scala tympani without causing physical trauma to the fragile intra-cochlear tissue membranes. It has been shown [33,34] that placement closer to the axially located spiral ganglion cells allows for decreased channel interaction between electrodes as well as lower stimulating thresholds. However, conventional electrode arrays are straight, and despite their flexible nature which allows them to curve somewhat to the physiology of the cochlea upon insertion they usually end up resting on the peripheral wall of the scala tympani. Recent designs have attempted to combat this by pre-curving the array in some manner, but the need to be straightened for insertions presents some issues. The Cochlear Contour Advance electrode array accounts for this by employing an internal stylet that straightens the array during insertion. As the array is advanced off the stylet and further into the cochlea its naturally molded curvature allows it to hug the modiolar wall. In similar fashion, the Modiolar Research Array [35] involves a rigid outer sheath to guide the electrode array through insertion into the first turn.

In addition to increased functional performance, guided arrays that hug the modiolus tend to avoid traumatic damage to the soft tissue membranes of the cochlea. Straight arrays required forceful contact with the lateral wall of the scala tympani to be directed around the spiral nature of the cochlea. Their flexibility leads them to often puncture upwards through the basilar membrane, in the same manner as the delaminating array of Fig. 4.3. To avoid this, a general principle that can be followed is to create arrays that are stiffer in the vertical plane to the direction of insertion than to the horizontal, thus minimizing upward bending [36]. Historically, trauma of some type has occurred in 10-20% of insertions regardless of array type

or surgeon skill level. This suggests that the manufacturer should assume imperfect insertion techniques and create arrays that can mechanically compensate by flexing in only the desired direction [37]. To further avoid tissue damage, arrays must avoid having sharp tips or edges that can easily tear or puncture membranes. The less traumatic the insertion is, the more likely any residual natural hearing ability can be retained. Mechanical flexing properties will be discussed further in Chapter 4.

Specific considerations related to electrode contact charge density must be taken into account when designing arrays. Extreme charge density at the interface between electrode contact and perilymph can lead to several negative side effects including tissue damage and excess scarring, contact breakdown and dissolution of metal ions, and irreversible generation of electrolysis byproducts such as O_2 or H_2 [38]. For these reasons it becomes necessary to reverse-engineer the contact sites, starting with the knowledge that typical currents required for intra-cochlear stimulation at maximum comfort (loudness) levels are on the order of 50-100 uA [38] [39] [40]. From here the amount of charge required per pulse can be determined, and then the electrode size necessary taking into account the specific material properties can be determined. This concept will be discussed further in relation to thin-film array electrode sites in Chapter 4.

3.3 Signal Processing Techniques

Although improvements in electrode array technology have been incremental in recent decades, signal processing techniques have undergone frequent and significant advancements as digital signal processing (DSP) capabilities have increased. The first cochlear implant introduced in section 3.1 included a very rudimentary analog processing unit that produced a single amplitude modulated signal. Audio picked up by a microphone was amplified, passed through a narrow bandpass filter, and fed to a 16 kHz modulator. This strategy meant that the total average energy of sound across the entire frequency spectrum was used to modulate the

amplitude of a single carrier wave, and that the patient only gained a sense of overall environmental loudness. Modern processors have drastically higher capabilities. As with most semiconductor chip based devices, cochlear implant speech processor development can be said to have in general followed Moore's Law of an exponential increase in capability over time. This is directly related to advancements such as processor speed and power efficiency increases of the embedded DSP chips which have led to increasingly sophisticated methods of conditioning the input audio signal.

Along with increases in hardware capability, our improved understanding of the way in which electrical impulses are coded into sounds allows us to deliver the most efficient pulse patterns to the auditory neurons. One of the most important advances in understanding is highlighted by the defining of Fine Structure (FS) information in a signal [41]. The FS component of a signal is defined as the carrier signal of its Hilbert decomposition and has been shown to convey significantly more detailed information than simple envelopes. Smith et al. performed perception tests that compared listener abilities to distinguish certain features of the same audio conditioned through standard envelope modulation and through FS-centric processing with Hilbert transforms [42]. The results showed that melody detection with fewer than 32 channels was only possible with FS processing, and that 48-64 envelope channels were required to attain the same results. FS information was also shown to be critical for speech recognition using fewer than 8 channels, and was almost exclusively responsible for sound lateralization abilities. MED-EL's Maestro processor employs a FS processing algorithm that enables enhanced ability to distinguish between close frequencies, and it is so effective that 92% of users report that music is pleasant to listen to [61]. The following are a few other selected processing developments that have had a significant impact in speech processor development.

3.3.1 Continuous Interleaved Sampling

Multichannel implants were a logical next step in the development of electrode arrays. Natural sounds are a continuous analog signal, so a discrete system that attempts to represent it will ideally be more accurate the higher the number of representation elements (electrodes) it incorporates. In multi-electrode stimulation neighboring electrodes can often interfere with one-another, so the continuous Interleaved Sampling (CIS) approach was created to allow for non-simultaneous stimulation of nearby electrodes [26]. In this approach, trains of bi-phasic pulses are delivered to the electrodes in a staggered manner such that no two electrodes are delivering current at the same time. The frequency, or pulse rate, that is delivered to the electrodes is high enough that the patient cannot detect any (unintended) temporal difference between activation of two different electrodes. Multiple studies [26, 27] confirmed that the CIS approach effectively decreased inter-electrode interference and allowed patients to score significantly higher on speech recognition tests.

3.3.2 Spectral Peak

A problem that has persisted throughout the entirety of cochlear implant development is the frequent inability of users to distinguish speech in noisy environments. One approach to solving this problem is the Spectral Peak (SPEAK) strategy developed by Cochlear, Ltd. (Cochlear, Ltd., Sydney, Australia). The input signal is filtered through a bank of 20 bandpass filters, the outputs of which are continuously estimated by the processor to determine the n ($5 < n < 10$) filter bands with the most information (maximum signal power) [28]. The stimulation rate is based upon the number of maxima selected, thus enabling quickly changing sounds with limited spectral content to be represented by only a few channels running at a higher pulse rate. This strategy represents an effective method for applying the DSP chip's full processing power in the highly dynamic trade-off between spectral and temporal representation.

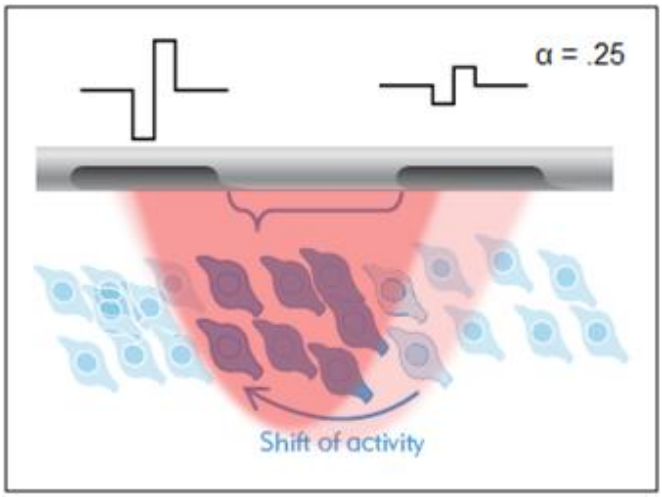

Fig. 3.2 An example of current steering between two electrodes. The "shift of activity" references a change in α from .5, where current is evenly distributed between the electrodes, to α = .25 and the left electrode has twice the current of the right. The significance of this is that a range of neural populations intermediate to two electrodes can be stimulated. [29]

3.3.3 Multipolar Stimulation

One approach to increasing the number of array electrodes available for stimulation is to employ multipolar stimulation techniques that create a virtual presence of intermediary electrodes. Current steering, employed commercially by Advanced Bionics (Advanced Bionics, LLC, Stafa, Switzerland) [29], is the practice of simultaneously stimulating neighboring electrodes so that they induce a maximum electrical potential at some point between the electrodes, dependent on the weighted current α of the secondary electrode [30]. Fig. 3.2 shows an example of current steering between two electrodes where α = .25. The "shift" referenced is from the previous state where α = .5 and each electrode contributed the same amount of current. Now that the left electrode is contributing twice as much current as the right, the region of activation has shifted towards it, although it is still activating a population of neurons that would not be activated by monopolar stimulation from either of the single electrodes. This stimulation pattern ideally leads to an intermediary pitch perception by the implant user as compared to either pitch heard by monopolar stimulation of the single electrodes.

A second multipolar stimulation approach incorporates current focusing, which uses negative current in the electrodes to either side of the target electrodes to narrow the pattern of positive neural activation. This technique serves to address the issue of widespread neural activation characteristic of a single electrode due to the fact that the electrodes are not placed directly on the target neurons, and the electromagnetic field expands as it gets further from the source electrode. Considering Fig. 3.2 again, current focusing would allow an electrode to activate a single column of neurons as opposed to the three activated columns shown in dark blue, thus creating a more focused and accurate pitch perception as intended by the sound processor.

3.3.4 A Multichannel Signal Processing Simulation in MATLAB®

To demonstrate the effects of increasing channel count on the quality of sound reproduction for cochlear implant recipients, an envelope modulation based simulation was created in MATLAB (see Appendix A for code) to reconstruct an idealized representation of how implant users perceive natural sounds. A GUI, shown in Fig. 3.3, was created to give users visual control over simulation parameters such as channel count and filtering strategy. Various graphs are used to display relevant information such as input and output signal power spectrums, filterbank frequency response, and envelope detection signatures. To generate a simulation, the user performs the following process through the GUI:

1) Load input audio file of type ".wav". This can be played back through the GUI.
2) Select the filter type. This algorithm implements infinite impulse response (IIR) filters, and the user can choose between Butterworth and Chebyshev type I or II methods.
3) Select the number of channels *N*. This theoretically represents the number of electrodes and separate frequencies an implant user would be able to discern. In practice, here it means the number of times the filtering operation is iterated and the number of pure sine waves used to form the output signal.

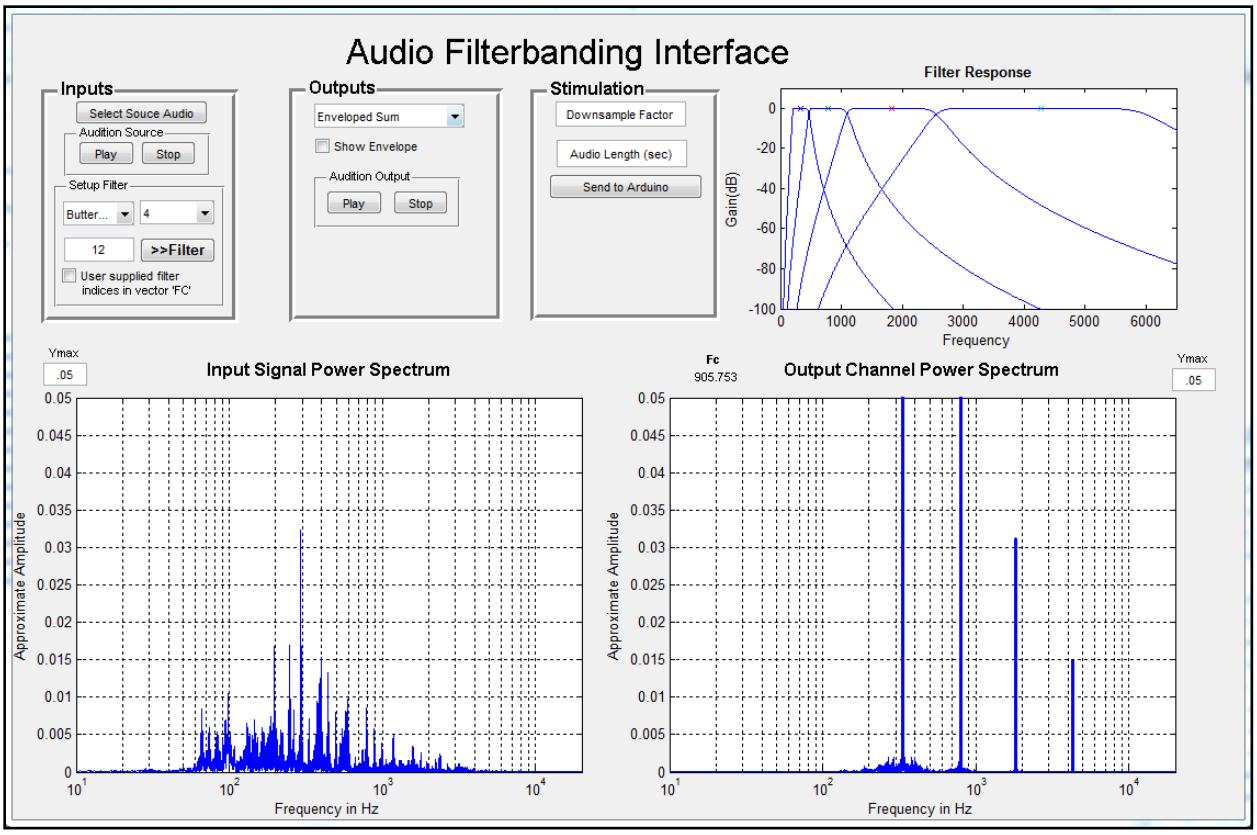

Fig. 3.3 The MATLAB GUI for the cochlear implant simulation code. The GUI contains input controls to allow for selection and playback of an audio file, filter parameters to customize the nature of the filterbank used to divide up the audio file, and output controls to display the power spectrum of the selected output channel. The GUI in its current configuration shows a 4-band butterworth filter of order 12 as it was applied to an audio file. The graph on the bottom left shows the power of the input signal, which is distributed naturally across the entire standard frequency spectrum. The graph on the bottom right shows the power of the output signal which has been limited to 4 narrow frequency bands corresponding to the center frequencies of the filterbank, whose frequency response is shown in the graph "Filter Response".

4) Select the filter order. Higher orders filters generate better separation between filter bands but become unrealistic due to complexity and processing power required in an actual hardware implementation.

5) Hit "Filter". A single band-pass filter is consecutively applied to the input signal *N* times, each time incrementing to a passband of higher frequency. The built-in algorithm spaces the bands logarithmically across the frequency spectrum, although the user can supply a custom vector of filter indices for more specific spacing. The filterbank frequency response shows up in the "Filter Response" window.

6) Select an output channel in the output dropdown menu to see the power spectrum of a single channel. Select the “Show Envelope” checkbox to see the envelope signal that is generated from that channel’s power spectrum. This envelope is then used to modulate the amplitude of a pure sine wave at the center frequency of the respective channel’s frequency band. Fig. 3.3 shows an example of an envelope signal.
7) Select “Enveloped Sum” from the output dropdown menu. The power spectrum of the simulated output is shown. In Fig. 3.3 you can see that the output signal effectively only has power at 4 single frequencies because $N = 4$ for the given setup.
8) Finally, the simulated output can be audition through the GUI to give an idealistic interpretation of what cochlear implant stimulation sounds like to an actual user.

This algorithm presents a highly idealized and simplified example of how cochlear implant processing works. For example, the center frequencies of the filterbands are in reality much more specifically determined as opposed to a simple logarithmic distribution. This is why the

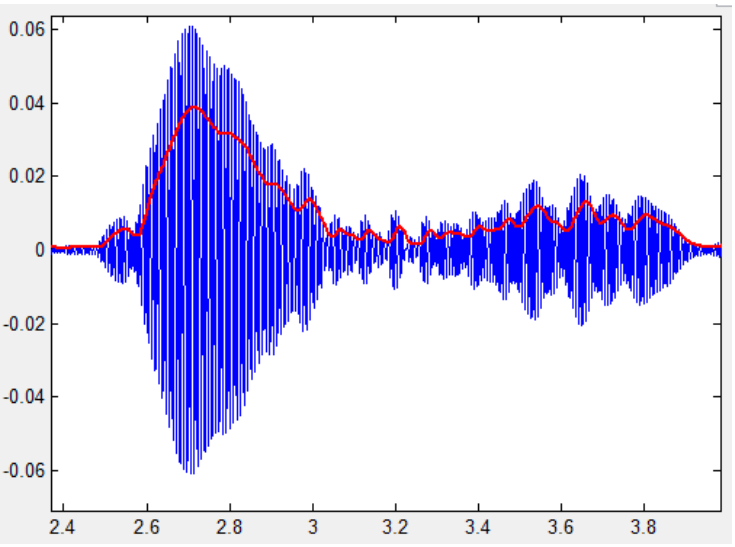

Fig. 3.4 The envelope (red line) associated with the power contained in the audio waveform (blue) of a single channel. The envelope is attained by full-wave rectification of the audio waveform and then low pass filtering. The cutoff frequency of the low pass filter determines how sharply the envelope follows amplitude changes of the original signal. In this simulator, the envelope is then used to directly modulate a pure sine wave whose frequency is equal to the center frequency of the respective filterband for the channel.

simulator allows the user to load in a custom vector of filterband cutoff frequencies so that channels can be effectively allocated to the most important parts of the frequency spectrum. The stimulation section of the GUI provides further abilities to interface with an external Arduino microcontroller to perform stimulations.

3.4 Commercially Available Technologies

An understanding of commercially available cochlear implant technology is fundamental to the process of seeking to create new designs. Table 3.1 outlines 4 leading commercially available devices and compares them in terms of relevant parameters. The maximum number of electrodes commercially available is 24, while the maximum electrode density is .8 mm. In order

Table 3.1 Implant technology from 4 leading manufacturers. The perimodular ability, electrode count, and electrode spacing are of specific importance to this work [43] – [50].

Manufacturer	Advanced Bionics	Cochlear Ltd.	MED-EL	Neurelec
Speech Processor	**Harmony HiRes Fidelity 120**	**Nucleus Freedom**	**Maestro**	**Saphyr SP**
Maximum Pulse Rate	83,000 Hz	32,000 Hz	50,000 Hz	24,000
Coding Algorithms	HiRes, CIS, MPS	ACE, CIS, SPEAK	FSP, HP-CIS	CRYSTALIS
Input Dynamic Range	80 dB	45 dB	55 dB	75 dB
Electrode Array	**HiRes 90K Implant**	**Contour Advance**	**Concert**	**Digisonic SP**
Array width (base to apex)	.7 to .45 mm	.8 to .2 mm	.7 to .5 mm	1.07-.5
Perimodular Array	Yes	Yes	No	No
Number of Electrodes	16	22	24 (12 channels)	20
Insertion Depth	23 mm	18 mm	31 mm	25
Electrode Spacing	1.1 mm	.8 mm	2.4	1.25
Multi Current Sources	Yes	No	Yes	No
Year Released Processor/Array	2007/2005	2005/2002	2011	2004

to investigate the potential benefits of high density electrodes this work seeks to improve upon both of these parameters. It is also important to note that two leading manufacturers have successfully functioning pre-curved arrays to attain closer proximity to the modiolus. This further motivates the desire to form a pre-curved electrode array as discussed in Chapter 4.

3.5 Barriers to Evolution

The previous section and the concept of increasing spectral representation of the implant introduce a major motivation for the experimental work presented in this paper. As mentioned above, commercially available implants have reached a plateau in terms of both electrode quantity and electrode density. The cochlear anatomy, specifically the height of the scala tympani, limits the number of electrodes by limiting the diameter of the electrode array. The obvious answer of decreasing lead wire diameter is not an ideal choice because it means increasing the electrical impedance to each site and therefore increasing the power required for the device to operate. Secondary to this problem is the fact that manufacturing techniques related to current electrode design limit the ability to make smaller, more tightly packed electrode arrays [38]. The signal processing and stimulation strategies mentioned above attempt to bypass these issues and create virtual intermediate electrodes, but testing and MATLAB® modeling [7] have shown that these techniques require significantly more power to operate. The remainder of this work will focus on the development and testing of a polyimide thin film array based electrode with a significantly higher site density than anything commercially available.

CHAPTER 4: ASSEMBLY OF A NOVEL IMPLANT

MEMS-fabricated polyimide thin film arrays (TFAs) present a novel approach to the idea of implantable intra-cochlear devices. They have much smaller implantation profiles while offering significantly higher electrode densities. However, due to their thin and flexible nature they present some unique barriers to surgical implantation, mainly because they lack the rigidity to be pushed into the scala tympani. Previous work [7] introduced the concept of bonding TFAs to clinically certified surgical backings, and while the methods showed promise functional testing revealed significant issues that this work aims to address in order to make TFAs a viable option for future animal and human studies.

4.1 Thin Film Array Technology

4.1.1 History of Thin Film Array Development

Silicon-based micro-electrode arrays (MEAs) introduced in the early 1980's delivered a way to interface with very specific, local populations of neurons for recording and stimulation purposes [52]. Although these initially bulky probes have been streamlined over the years, the structural rigidity of silicon makes these devices poor solutions for many applications. Cortical surface interfacing, which requires a more flexible array, is one such application. Issues commonly arose involving "cross-walking" of the rigid silicon based arrays through the soft target neural tissue because of extreme differences in material properties [53]. Not only does this lead to inconsistent neural recordings, but it also increases tissue damage, inflammation, and resulting scar tissue. Researchers in this and related fields began investigating the use of polymer-based thin-films to allow for the creation of flexible arrays that could still be manufactured with standard IC fabrication techniques, thus retaining the small feature sizes of

traditional silicon based arrays. Specifically, they needed a polymer substrate that was etchable and would adhere to commercially available photoresists to utilize photolithographic techniques [38]. Formally, the requirements for an ideal polymer are as follows:

- Biocompatible, bio-stable, and chemically inert
- Mechanically flexible
- Insoluble in and impermeable to the ions of the perilymph
- Low dielectric constant to reduce capacitive leakage and electrode cross talk
- Freedom from pinholes and other mechanical defects
- Good metal adherence for contact deposition
- IC process compatibility: Photolithography, CVD, Metal Sputtering, etc.

These constraints led to the testing of various polymers including poly-dimethylsiloxane, parylene, polyimides, and benzocarbonates [54]. Among these, members of the polyimide family showed the most promise.

4.1.2 Polyimide as a Thin Film Substrate

Aromatic thermosetting polyimides show use as thin-film array substrates for cochlear implants as far back as 1982, and have been available for use in other commercial processes dating to 1955 [38]. Polyimides were initially considered because they have good dielectric characteristics (insulator resistance and low dielectric constant) comparable to other commonly used materials in silicon technology such as SiO_2 and Si_3N_4 [55]. For example, the dielectric constant of SiO_2 is 3.9 and that of polyimides is 3.4 while also having a lower density. The first example of polyimide use in TFAs employed Pyralin PI-2555, but other variants have been used as the application requirements were refined. Table 4.1 shows commonly used Pyralin precursors and selected important characteristics. This table, taken from data compiled in 2000, involved research that focused on the PI-2611 variant which was chosen for its biocompatibility

Table 4.1 Material Properties of Different Polyimides. Although PI-2611 has the least favorable Young's Modulus for matching tissue characteristics, it was shown to be the most biocompatible [55].

Precursors	Kapton PMDA/DADE	PI 2556 BTDA/ODA/MPD	PI 2566 6-FDA/ODA	PI 2611 BPDA/PPD
Sheet thickness [um]	7.5 - 125	0.5 – 1.5	1.3 – 2.2	5.0 – 10.0
Water uptake [%]	4	2 – 3	1.5	0.5
Elongation [%]	25 – 50	15	12	25
Density	1.42	1.45	1.06	1.07
Resistivity [Ω – cm]	10^{17}	$> 10^{16}$	-	$> 10^{16}$
Dielectric Strength [V/cm]	$1.1*10^{6}$	$2*10^{6}$	-	$2*10^{6}$
Young's Modulus [kg/mm^2]	255	245	175	845

characteristics compared to the others. For example, although PI-2566 showed higher transparency and adhesion characteristics, it is fluorinated and thus shows only medium biocompatibility in cytotoxicity tests [55].

To date, polyimides have been extensively studied for use as substrates in thin-films for neural interfacing applications. Their excellent mechanical properties, biocompatibility, and stability in wet microfabrication processes have proliferated their use in applications including the study of brain slices in vitro, recording of cortical action potentials, and interfacing with regenerating peripheral nerves [54]. A useful property of polyimides is that they can be solidified with an initial curing heat treatment, but remain chemically active and susceptible to photolithography masking and etching until a final high temperature cure is performed. Finally, an important consideration is that polyimides more closely match the material properties of neural tissue as compared to the original silicon MEAs mentioned above. They have a Young's Modulus on the order of 3 GPa whereas silicon and brain tissue are 170 GPa and 3kPa respectively. Thus, polyimide use reduces the mechanical impedance mismatch at the material interface.

The material used for electrode contact sites in TFAs has also been extensively investigated as well, and noble metals such as platinum and iridium have emerged as the most

viable options. Noble metals are resistant to the deteriorating effects of oxidation and corrosion in moist environments, a quality that is obviously critical to the long term stability of implantable electrode contacts. Although charge transfer between an electrode and the perilymph can be purely capacitive, the intra-cochlear current required for auditory nerve activation requires significant charge transfer at the interface, thus creating the potential for irreversible side effects from faradic reactions. Trace analysis of solutions after Pt electrode stimulation by Brummer et al. not only showed that Pt was stable enough for use in stimulating applications, but also characterized the galvanic degradation of the material at high charge densities and concluded that Pt can handle a maximum charge of up to 300 $\mu C/cm^2$ [40]. This knowledge allows us to better estimate the proper electrode surface area for a given application according to the required currents. Returning to the design process introduced in section 3.2.2, consider the decisions described by Shamma [38] in determining electrode size. They chose a maximum charge density required for stimulation to be 100 nC per pulse phase. Using Pt with a maximum charge density of 300 $\mu C/cm^2$ and pulse durations of 200 µs leads to a minimum electrode area of .001 cm^2, or 300 µm x 300 µm.

In addition to platinum, iridium is frequently added to electrode material in ratios of approximately 90% Pt – 10% Ir to generate alloys with increased tensile strength [39]. Overall, an overwhelming number of studies over the past decades have proven the long term stability of Pt-Ir electrodes in vivo, and more recent studies have confirmed the biocompatibility of polyimide based arrays with platinum electrode sites [54],[57]. Despite polyimide's continued successes, certain applications require further optimization of the material for use as an implantable interface.

4.2 The Basis For Improvement

This section introduces the previous work on combining polyimide TFAs with surgical backings, first discussing the various components we employ and then highlighting the areas for improvement. An experimental procedure by Stephen Rebscher of the Department of Otolaryngology at the University of California, San Francisco is also introduced as a method to quantify the mechanical performance of an electrode array.

4.2.1 Components

Thin-film polyimide arrays (TFAs) were fabricated by NeuroNexus (NeuroNexus, Ann Arbor, Michigan, USA) to custom specifications. The arrays used in this work, shown in Figs. 1 & 4.2 A, are 32 mm long and feature twenty-one 180 µm diameter platinum sites with a center spacing of 250 µm placed over the tip-most 5.5 mm of the array. This work concerns two versions of the arrays, one that has an electrical connector at the base and is considered "electrically active", and another "dummy" that has no connector. Both arrays have identical mechanical properties.

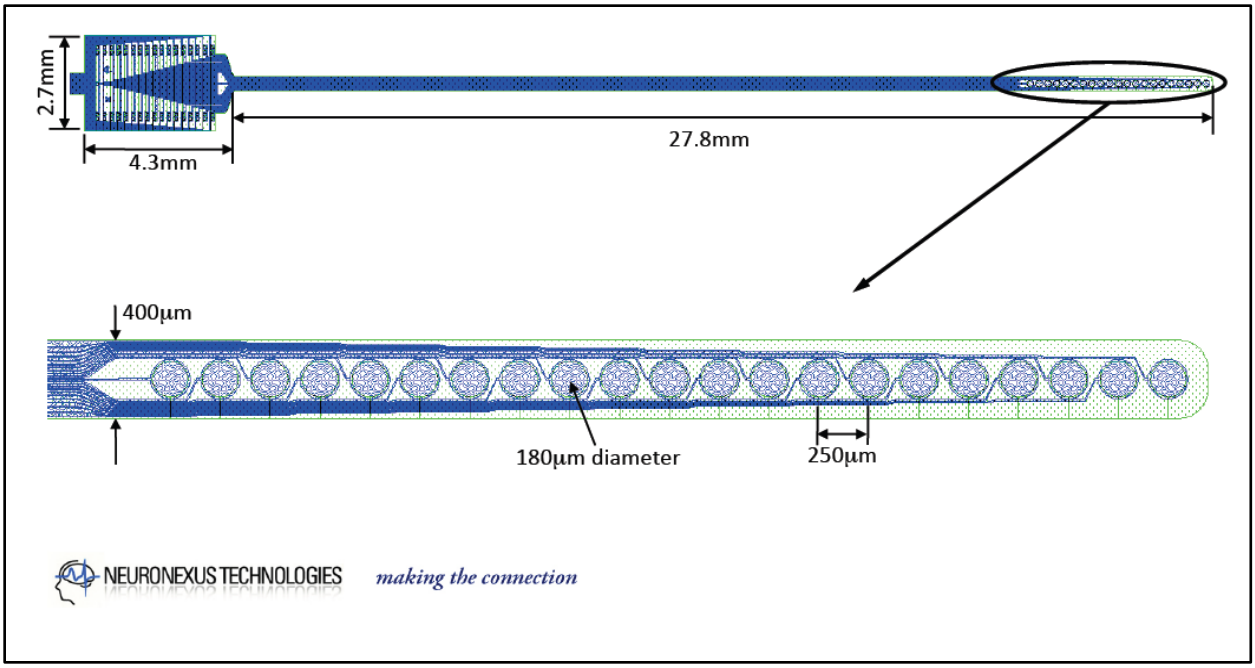

Fig. 4.1 Schematic of the 21-site thin film arrays custom designed by NeuroNexus

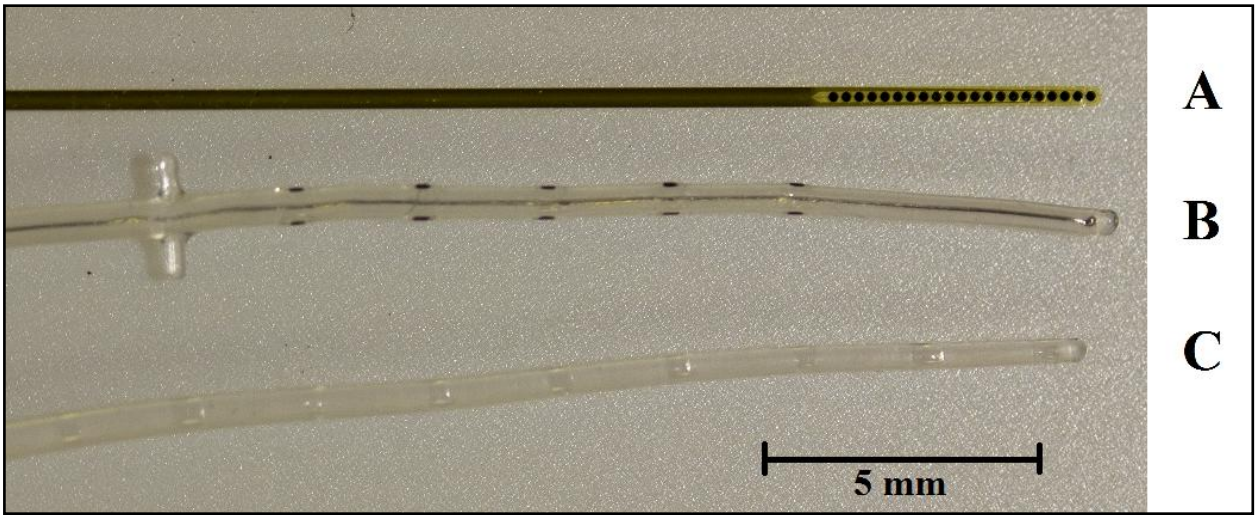

Fig. 4.2 Comparison of the elements used in the following assembly procedures. (A) NeuroNexus polyimide Thin Film Array showing the 21 platinum electrodes; (B) MED-EL silicone based Insertion Test Device. The wire core and black insertion distance markers are visible; (C) MED-EL Insertion Electrode, a silicon dummy array without electrodes or lead wires

Insertion Test Devices (ITDs) shown in Fig. 4.2 B were supplied by MED-EL (MED-EL Corporation, Innsbruck, Austria) as a potential backing to be bonded to the arrays. ITDs are clinically certified for use in patients to verify depth of access to the scala tympani before implantation of an electrode. They are molded silicone with a wire core that adds selective rigidity in the vertical plane. Another key characteristic of the ITD is a “T-stopper” that lets the surgeon know when he has reached the maximum necessary insertion depth.

Insertion Electrodes (IEs) shown in Fig. 4.2 C are also supplied by MED-EL. These are molded silicone dummies and are prepared in the same mold as actual MED-EL electrode arrays but they contain no electrodes or internal wires, thus they are more flexible than ITDs. Collectively, the IE and ITDs are referred to as **Insertion Platforms (IPs)**. Table 4.2 provides a summary of the various component properties.

Table 4.2 Comparison breakdown of the various features of the TFA and IPs

	TFA (Thin-Film Array)	ITD (Insertion Test Device)	IE - C40 Dummy (Insertion Electrode)
Length	- 27.8 mm - electrodes on tip-most 5.5 mm	- 120 mm - T-stopper 17.8mm from tip	- 134 mm -31.5 mm to raised ring marker
Diameter	- 0.4 mm constant width - 0.02 mm constant depth	- 1.3 mm at base - 0.7 mm at T-stopper - 0.5 mm at tip	- 1.3 mm at base - 1.3 mm at ring - 0.5 mm at tip
Structure	- Polyimide substrate - Twenty-one 20 Å Platinum sites	- Silicone body - Pt-Ir wire core (.1 x .04 mm)	- Silicone body only
Notes	Two types used: one has an electrical connector socket and is functionally active, the other is just	- 2.4 mm spacing between markers	normally would have embedded Pt-Ir electrodes and wires

4.2.2 Previous Development and Improvements

The original work [31] attempted straightforward bonding of TFA's to ITDs using silicone RTV adhesive which resulted in various types of assembly and insertion errors. Fig. 4.3 shows a cross section of one of these assemblies after insertion into a human cadaver cochlea, where the white structure is the cross section of the ITD and the gold ribbon is the TFA. As this image shows, the TFA has delaminated from the ITD and the sharp tip has penetrated the basilar membrane and now resides in the scala vestibuli. It is important to note that the TFA's used in this preliminary work were of a much smaller profile, having a length of only 12 mm and a width of 196 µm, although their adhesive and mechanical flexibility properties are comparable with those of the TFA's used in this work. In general, we hypothesize that weak adhesion of the silicone glue to the TFA allowed the array to become delaminated at the tip or anywhere along

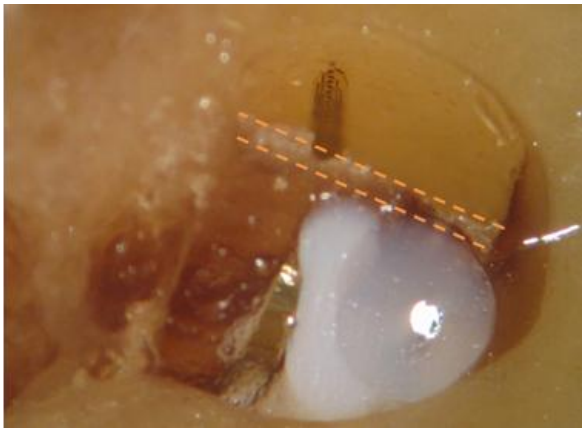

Fig. 4.3 Histological Cross section of an inserted assembly showing TFA (gold ribbon) delamination from the IP (white body) and excursion through the basilar membrane (outlined with orange dotted lines).

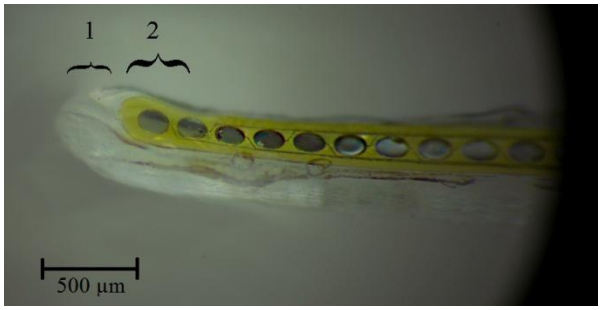

Fig. 4.4 The tip section of a 2nd generation assembly includes a second layer of silicon adhesive on top of the array tip to lock the tip down (region 2). The array tip is also recessed slightly from the ITD tip (region 1) to help prevent delamination or puncturing of the basilar membrane.

the bonding, and also allowed the array to kink when the assembly bent following insertion. To summarize, issues revealed in the preliminary study that this work aims to address include:

- Array tip delamination allowing excursion into the scala vestibuli
- Overall weak bonding leading to general delamination and kinking
- Severe array kinking resulting from “straight” assemblies being bent upon insertion through the curvature of the cochlear first turn

Several measures were undertaken in this study to combat these issues, the first of which was the application of an additional glue coating to reinforce the assembly. The original study laid out the ITD flat and straight, applied a thin layer of NuSil (NuSil Silicone Technology LLC, Carpinteria, CA) MED-2000 silicone RTV adhesive using a digitally controlled dispensing system, and then laid the array on top of that. Because of the nature of the array’s smooth surface, the silicone glue does not adhere to it well and the array can thus peel off quite easily. To structurally reinforce the next iteration of assemblies, a second layer of glue was added on top of the array, effectively encapsulating the array in the adhesive. Special care was taken to avoid covering the array at the electrode sites through the use of visual inspection through low

powered magnification during the gluing process, and also by using a highly controllable digital dispensing system for the adhesive The next measure taken to combat delamination issues was to cover the tip-most electrode with a second layer of glue to ensure that tip delamination does not occur. While this does render that electrode non-functional, future iterations of arrays will account for this and leave some dead space at the tip during fabrication. Also to avoid tip delamination, the array was recessed in relation to the ITD about ½ mm so that the soft tip of the ITD makes contact with the cochlear wall during insertion as opposed to the sharp tip of the array, which has the potential to puncture the basilar membrane. See Fig. 4.4 for the improved tip structure.

4.2.3 Mechanical Properties and a Quantification of Vertical versus Horizontal Stiffness

The mechanical properties of a cochlear electrode array directly correlate to the amount of trauma that is likely to induce upon insertion into the scala tympani. For this reason it is important to consider the specific mechanical properties of each component involved in our devices. The TFAs are extremely flexible and cannot cause much harm through compressive contact force with another surface. However, the array has an extremely sharp, thin tip and edges, and when coupled to some type of rigid insertion device can effectively become a dangerous “spear-like” hazard to the soft tissue membranes of the cochlea. IEs and ITDs on the other hand are composed of soft silicone and do not have sharp edges, but their increased rigidity allows them to deliver compressive forces to tissues they encounter. It is important to remember that ITDs do have a thin wire core that decreases their overall flexibility, and makes them more selective to flexing in one plane.

Table 4.3 shows a comparison of the mechanical properties of several commercially available and prototype arrays and the resulting trauma from an insertion study performed by Rebscher et al. [36]. In this test, array flexibility was determined by measuring the amount of force, in grams, that was required to deflect the array 30º by applying pressure 2mm from a

pivot point. This procedure was repeated along the apical 6mm of the array, and in both the horizontal and vertical orientations. Although the results are somewhat variable, a correlation (r = -0.83) between increased vertical stiffness and reduced trauma can be seen. These results show a new perspective on methods for reducing insertion trauma, and provide a point of reference for evaluating the stiffness of our arrays. Additionally, previous FEM analysis has shown that wire-core electrode arrays with the lead wires arranged such that the Young's Modulus is higher in the horizontal plane versus the vertical plane require higher insertion forces and result in greater contact pressures with the lateral wall of the cochlea [63]. Although results of the benefits of increased horizontal flexibility in literature are currently limited, these experimental and simulated results provide a basic motivation for evaluating the preferential flexibility of our fabricated electrode arrays. While we would not want to purposely increase the vertical stiffness of an array beyond standard ranges for the sake of making it comparatively more flexible in one direction, decreasing overall stiffness while keeping in mind preferential flexing could be beneficial. Considering that our array components do not involve wire cores (disregarding the single thin core of the ITD), we anticipate an overall decreased stiffness and a

Table 4.3 Trauma and insertion depth results comparing the preferential stiffness of various commercial and prototype electrode arrays. Of important note is the correlation between V/H force ratio and Trauma, which showed a correlation coefficient of -.83. This indicates that increased stiffness in the vertical direction does in fact aid in avoiding trauma. The outlier, HF II with position > 400° could be explained by the deeper insertion depth and greater chance of impacting membranes in the narrower apical region. [36]

Electrode Array	Vertical Force (g)	Horizontal Force (g)	Mean Force (g)	V/H Force	Trauma in Scala Vest.	Mean Depth
Cochlear Banded	0.50	0.70	0.60	.71	37.5%	285°
Spiral Clarion	3.27	2.92	3.09	1.15	0.0%	445°
Cochlear Contour	1.33	1.97	1.65	0.68	38.9%	417°
HF II with pos < 400°	1.29	0.47	0.88	2.77	0.0%	332°
HF II with pos > 400°	1.29	0.47	0.88	2.77	66.6%	508°
Contour Advance	1.33	1.97	1.65	0.68	33.0%	367°
Neurobiosys	1.03	0.58	0.80	1.77	0.0%	360°
Helix Exprmnt #1	3.58	1.28	2.43	2.79	0.0%	390°
Helix Exprmnt #2	3.29	1.23	2.26	2.67	10.0%	416°

potentially more horizontally flexible array due to the profile of the TFA. Chapter 5 will review modeling in simulation and physical testing to determine the actual nature of our arrays.

4.3 The Assembly Mold

While the initial changes mentioned above solved a majority of the tip delamination issues as evaluated by test insertions into a clear acrylic mold of the cochlea (see Fig. 4.10 for an example), the array still kinked upon insertion into the mold. This kinking is a result of the fact that the assembly dries in a straight position and is then required to curve to match the anatomy of the scala tympani upon insertion. The layers of the assembly cannot slide freely against each other during the bending process, forcing the array to fold up and away from the ITD and thus mechanically forcing delamination. This hints that the original approach to creating the assembly is structurally incapable of functioning effectively as an implant, and a new procedure involving a machined mold was developed to allow the assembly to cure in a curved position. While it is important for the assembly to be able to rest in a curved position inside the cochlea without array kinking or delamination, it is equally important that the assembly can be bent to a nearly straight orientation for initial insertion through the round window or the hole of a cochleostomy. For these reasons the mold radius of curvature was chosen to be 7/32”**,** an intermediate arc between straight and the curvature of the human cochlea.

The mold, shown in Fig. 4.5, was then fabricated out of type 6061 Aluminum using the Georgia Tech machine shop mills, lathes, and water jet cutter. The mold is made up of two main structures, a base labeled (2) that holds the IP in place and a hinged door labeled (1) to which the array is fastened using a clamping mechanism and suction. The bolts and Teflon screw on the door fasten the clamp, shown again in Fig. 4.6. The selective tightening of these fasteners allows for precise placement of the array along the door edge shown in close-up in Fig. 4.6.

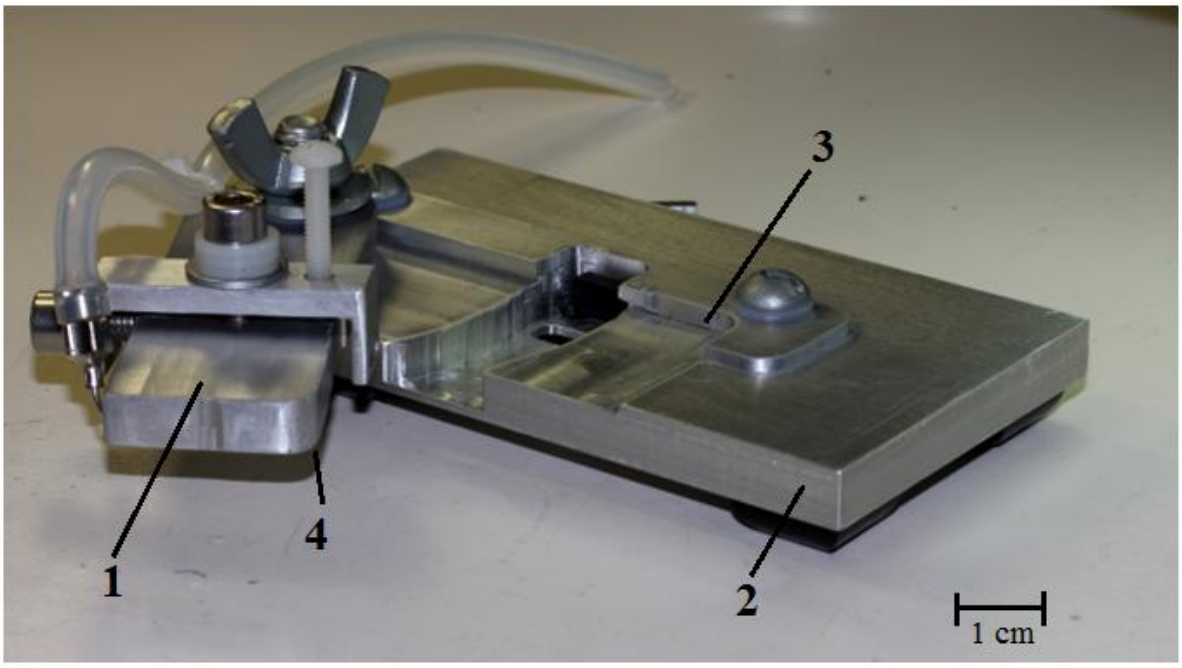

Fig. 4.5 Full view of the mold, machined out of 6061 Aluminum and coated with 15 microns of Parylene. The labeled elements include the “door” (1), the “base” (2), the groove where the IP lays (3), and the door edge where the array is fastened (4). The silicone tube leading off the top attaches to a suction pump which delivers the force necessary to temporarily secure the array tip as shown in Fig. 4.6.

Initial attempts at assembling TFAs to IPs failed because the silicone adhesive stuck to the bare aluminum mold. To account for this, a 15 micron parylene covering was applied to the mold using a chemical vapor deposition process. This layer serves as both a mold release and a hermetic seal to the underlying aluminum. In addition to this, following earlier work [32] with releasing silicone implants from stainless steel molds, a layer of 10% dish soap solution (Ajax Liquid Dish Soap) is applied to edges (3) and (4) of Fig. 4.5 to further discourage bonding of the silicone adhesive with the mold.

4.4 The Molding Process Outlined

The following procedure describes the specific steps that are followed when molding a TFA to an ITD or IE:

1) All parts of the mold are assembled, including all positioning and tightening bolts.
2) A layer of 10% dish soap solution (Ajax Liquid Dish Soap) is applied with a cotton-tipped applicator to the mold surfaces labeled (3) and (4) of Fig. 4.5 where the array and IP lay. This is left to dry for about 10 minutes while the following steps are performed.
3) An IP is removed from its packaging and placed on a glass slide. If using an ITD, ½ of the T-stopper must be cut off with a razor blade so that the array can lay flat against it. If using an IE, this step is not necessary.
4) A TFA is selected and cleaned with Acetone to remove all residues that might inhibit bonding with the silicone glue.
5) The TFA is attached to the door of the mold. First the array base is clamped down, and then the tip is maneuvered onto a small hole along the curve of the mold door which is connected to a pump and suctions the tip down. Fig. 4.6 shows a close up of the array in this position.
6) The IP is laid along the inner curve of the mold base, and using tweezers is pressed under the slight ledge (visible in Fig. 4.7) to be held in place.
7) A #25 plastic needle tip is filled with NuSil MED-2000 Silicone RTV adhesive (lot no. 55194). This is placed on the end of a syringe connected to a Madell Digitally Controlled pneumatic dispenser system (Madell Technology Corp., Ontario, CA).

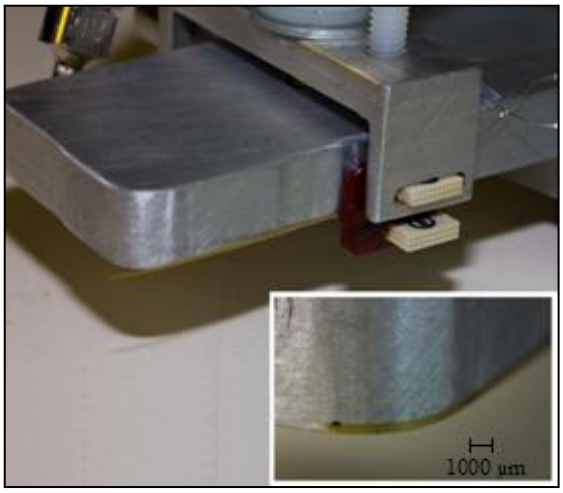

Fig. 4.6 Mounting of TFA to the door of the mold. First, the TFA's connector base, shown in dark red, is clamped down. Then the array tip is positioned over a tiny hole, shown in the inset, which is connected to a vacuum that holds the array tip in place via suction.

Fig. 4.7 Applying the first layer of Silicon Adhesive to the IP. Note how the IP is held in place by being gently wedged under the overhang of the curvature.

8) Once steps [5-7] have been satisfactorily performed, a layer of glue can be dispensed on the IP using a dispensing pressure of ~30 psi and interval times of 4-8 seconds, depending on preference.
9) After the glue has been laid down, the door is quickly but carefully closed into the base, sandwiching the array onto the glue + IP. Suction holding the array tip down must be **immediately** turned off to avoid clogging the channel with glue. The door wing nut is fastened and the assembly is left to dry for 24 hours.
10) Once dry, the mold piece clamping the array base to the door is removed. Now that the clamping and suction are gone, the array is no longer attached to the door, but it must now be secured to the base to prevent shearing of the array while the second glue layer is added. This is accomplished by using a clamp that comes up through the bottom of the base, as shown in Fig. 4.8.

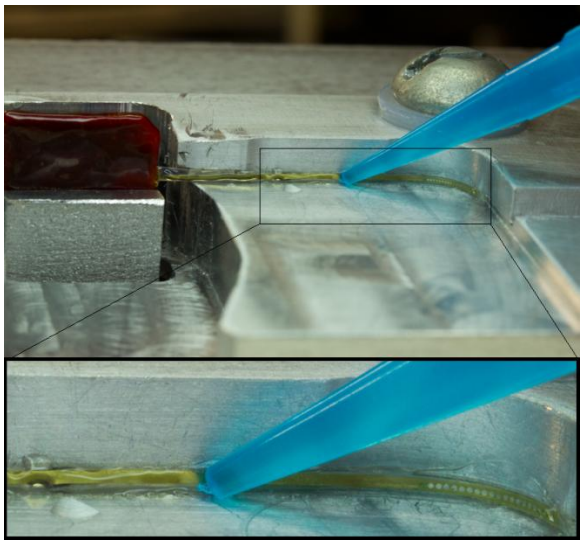

Fig. 4.8 The TFA is now clamped to the base, and the door is removed. A second layer of Silicon Adhesive is applied over the array, except where the electrodes are, to help secure it to the IP.

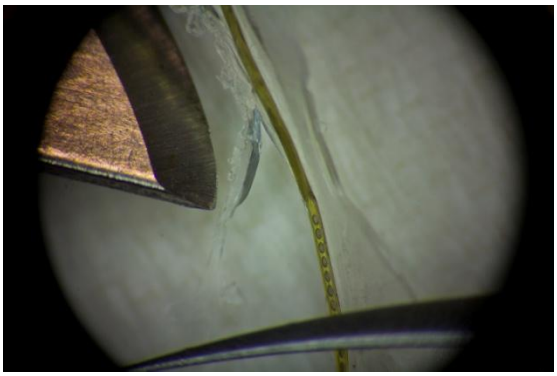

Fig. 4.9 Removing excess silicon adhesive "flanges" from the molded assembly is critical for ensuring that the final product is thin enough to be implanted through the first turn of the cochlea.

11) Once the array is re-secured, the door can be slowly opened. After opening the door a few millimeters, check to see if the assembly is sticking to the door or the base. If sticking to the door use fine tweezers to peel off and push back under the curve ledge from step [6]**.**
12) Once the door is fully removed, repeat step [7] and then apply a second *thin* layer of glue on top of the array, covering it everywhere except over the active sites as shown in Fig. 4.8. Also cover the tip, including the tip-most electrode as shown in Fig. 4.4.
13) After drying for 24 hours, remove the assembly from the mold completely and place on a clean glass slide. The assembly will have "flanges" of residual dried glue that must be removed.
14) Using a low powered binocular microscope and a curved Xacto knife, trim away the excess glue along the array as in Fig. 4.9. Be sure to trim away sharp edges or bumps that could engage the fragile tissue of the cochlear pathways.
15) Inspect the assembly for any areas needing tweaking with additional glue or trimming.

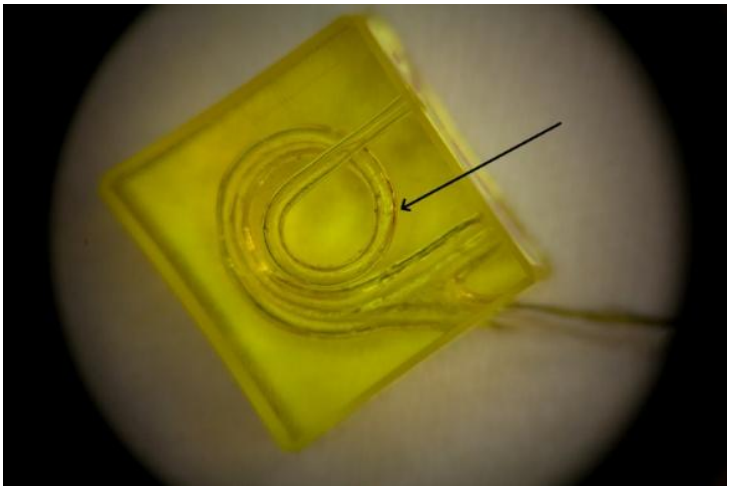

Fig. 4.10 Test insertion of the completed assembly into a cochlear model (courtesy of MED-EL). Although difficult to see, the arrow indicates the insertion depth of the IP, which is right at the target of 270°.

16) Once satisfied, test insert the finished assembly into the mold as shown in Fig. 4.10 to ensure that it is thin enough along the entire insertion length to fit in the cochlea.

4.5 Notes on the Molding Process

The process outlined above was refined over weeks of trial and error. Table 4.4 shows an overview of bondings that were attempted and resulting changes that were to the process.

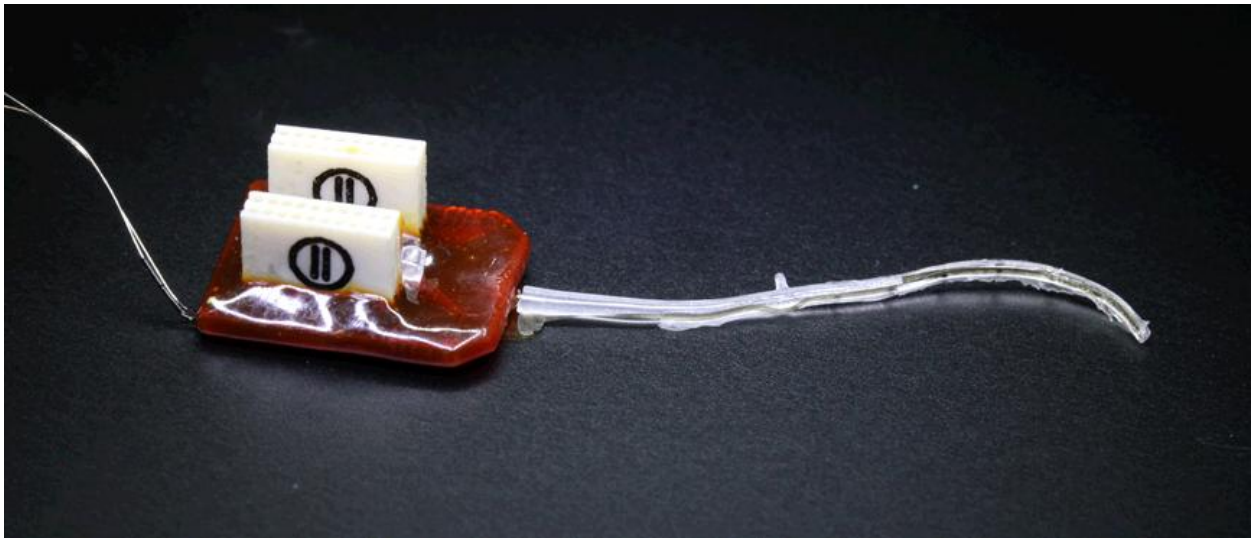

Fig. 4.11 completed assembly of an electrically active array with connector and ITD – notice the t-stopper sticking up in the middle of the array, indicating the point of full insertion.

Table 4.4 Assembly history, including changes made to process as a result of attempt outcomes. Note that the "optimization" of the mold for arrays with connectors does not negatively affect its performance when dummy arrays are used.

Assembly Description	Attempts	Delaminations	Notes
ITD+TFA, formed using hot wax and tweezers as per instructions of previous study	1	1	initial improvements to original system: addition of second layer of adhesive to tip and basal end, tip recessed on IP. Stopped using wax.
ITD+TFA, clamped with glass slides during adhesion. Second glue layer	2	1	Improvement, although delamination from kinking still occurs, even under second adhesive layer. Curved mold machined.
ITD+TFA, held in aluminum mold	1	NA	Silicone adhesive sticks to mold, investigated mold releases and added parylene coating to mold.
ITD+TFA, 10% soap solution on mold	2	1	Delamination occurred when trying to remove excess glue. Purchased curved razor blades.
ITD+TFA	5	0	Process optimized for IPs and dummy arrays.
IE+TFA	4	0	IEs present no additional challenges to process. Are easier to manipulate.
ITD+TFA+Connector	1	1	Delamination/array shearing when connector was detached from the door. Added additional clamp on base to secure connector during second adhesive layering
IE+TFA+Connector	2	0	Process optimized for including array connector.

While the mold is currently highly effective, certain issues had to be overcome during its development. Repeated trips to the machine shop were made to tweak the mold so that it was of the correct dimensions to properly hold the array and IP. Because the silicone adhesive bonds well to rough aluminum, the entire mold required a 15 micron layer of parylene coating, and then a 10% soap solution must be applied each time to relevant areas to ensure that the

dried glue releases easily from the mold surfaces. The mold was also initially designed to hold arrays with electrical connectors attached to them, and the clamping system is intended to fit around the connector. For this reason it takes a bit of delicate work to clamp down an array without a connector and then get the tip in proper alignment to be suctioned down. For an array with a connector, the clamp simply goes over the connector as shown in Fig. 4.6 and the position is quickly micro-adjusted with positioning screws.

Finally it is important to note the impact of the differences between the two types of IPs used thus far. The ITD's are meant to be inserted into the cochlea before an actual implant is inserted, and they have a central wire that adds some degree of rigidity. The IE's are dummy implants and are purely silicon, thus they are less rigid. They also do not have a T-stopper so one has somewhat more leeway when positioning it in the mold. For the cadaver verification study described in Chapter 5, four assemblies were made with ITD's and six with IE's. All came out well, but the IE's seem to be less likely to experience the delaminating forces of kinking and are in general easier to handle. They are also less likely to want to "push" themselves out of the cochlear mold once inserted. At this point it is assumed that these properties are directly related to their lack of internal wire and resulting increased flexibility, and it would be desirable to continue future work using IE's exclusively.

CHAPTER 5: FUNCTIONAL VALIDATION

Thus far it has been hypothesized that the functional abilities of a cochlear implant electrode array can be enhanced by both decreasing the electrode distance from the modiolus and by increasing selectivity to flex in the plane horizontal to the plane of insertion. Modiolar placement could lead to increased electrode selectivity and decreased stimulation currents while resistance to bending in the vertical plane helps avoid damage to and puncturing of the basilar membrane. In order to verify that our components and the assembly process outlined in Chapter 4 contribute to these properties, simulative and physical tests were performed to determine electrode performance. These tests were based largely on the procedure by Rebscher et al. in a 2008 study comparing various properties of 8 commercially or clinically available electrode arrays [36] as introduced in Table 4.3 of the previous chapter. Rebscher quantified each electrode by its ratio of average vertical to horizontal stiffness and showed that increases in this ratio led to decreases in insertion traumas.

5.1 COMSOL Modeling

5.1.1 Simulation Setup

Finite-element modeling of both types of assemblies as well as their individual components was performed in COMSOL 4.2a (The COMSOL Group, Stockholm, Sweeden) to validate the theoretical basis for selective flexing in the horizontal plane. Solid Mechanics Module simulations also revealed that during flexing, differential strain is at a maximum at the interface between the TFA and the IP, thus providing a theoretical basis for the delamination seen during insertions. Material properties, shown in Table 5.1, were input manually for the various components, with each requiring a value for density, Young's Modulus, and Poisson

Table 5.1 Relevant material properties for simulated materials. A comparison of Young's Moduli reveals that it should be the polyimide and platinum which dominate the flexibility characteristics of an assembled electrode. [34], [58], [59], [60]

Material	Density [kg/m^3]	Young's Modulus [kPa]	Poisson Ratio [1]
Polydimethylsiloxane (Silicone)	970	750	0.5
MED-2000 RTV Silicone Adhesive	923	360	0.5
Polyimide	1420	2,500	0.34
Platinum	21450	168x10^6	0.38

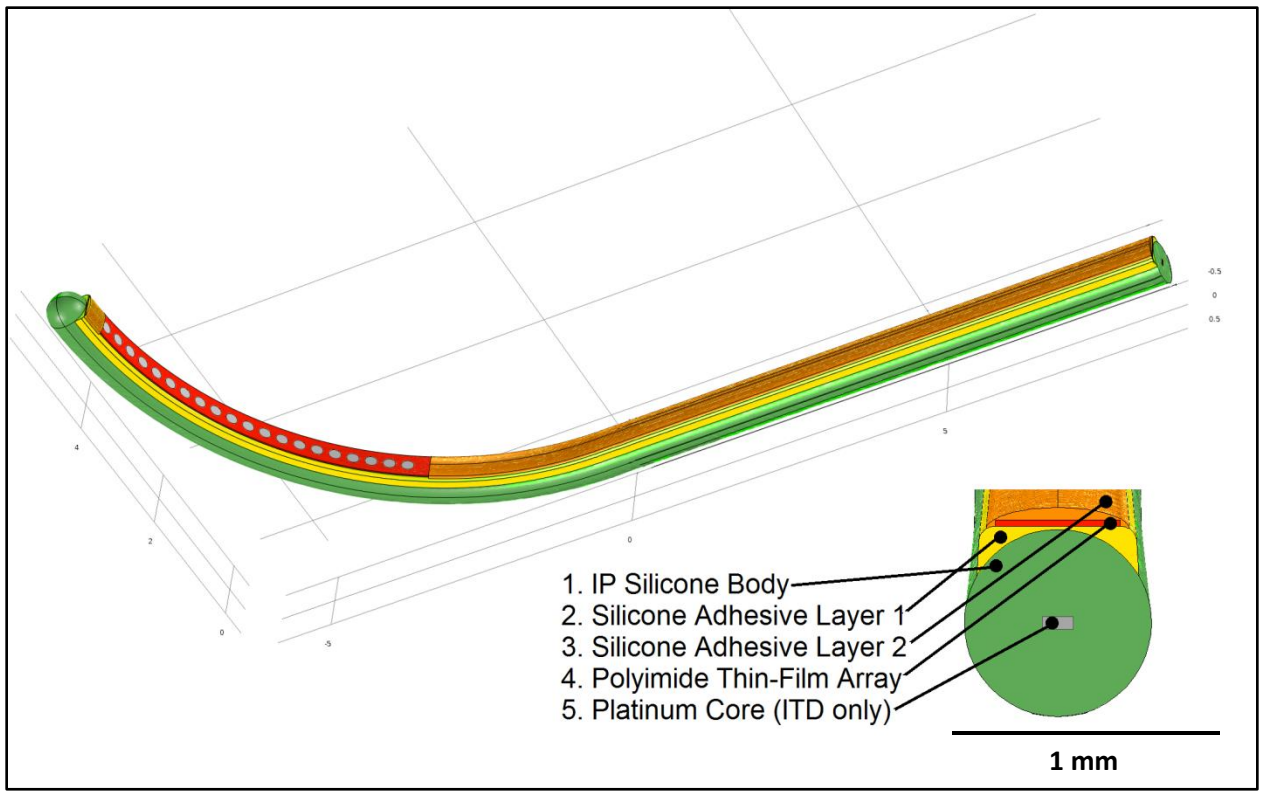

Fig. 5.1 Overview of the COMSOL assembly elements: IP-green (ITD with Pt core), first glue layer-yellow, TFA-red, second glue layer-gold, electrodes-silver. Note tip adhesive, which covers the first electrode.

Ratio for the Solid Mechanics solver in COMSOL. The Young's Moduli for polyimide and platinum are orders of magnitude higher than those of the silicone components, so it follows that the TFA and Pt core dominate the assemblies' performance in simulation. The modeled assembly with labeled components is shown in Fig. 5.1.

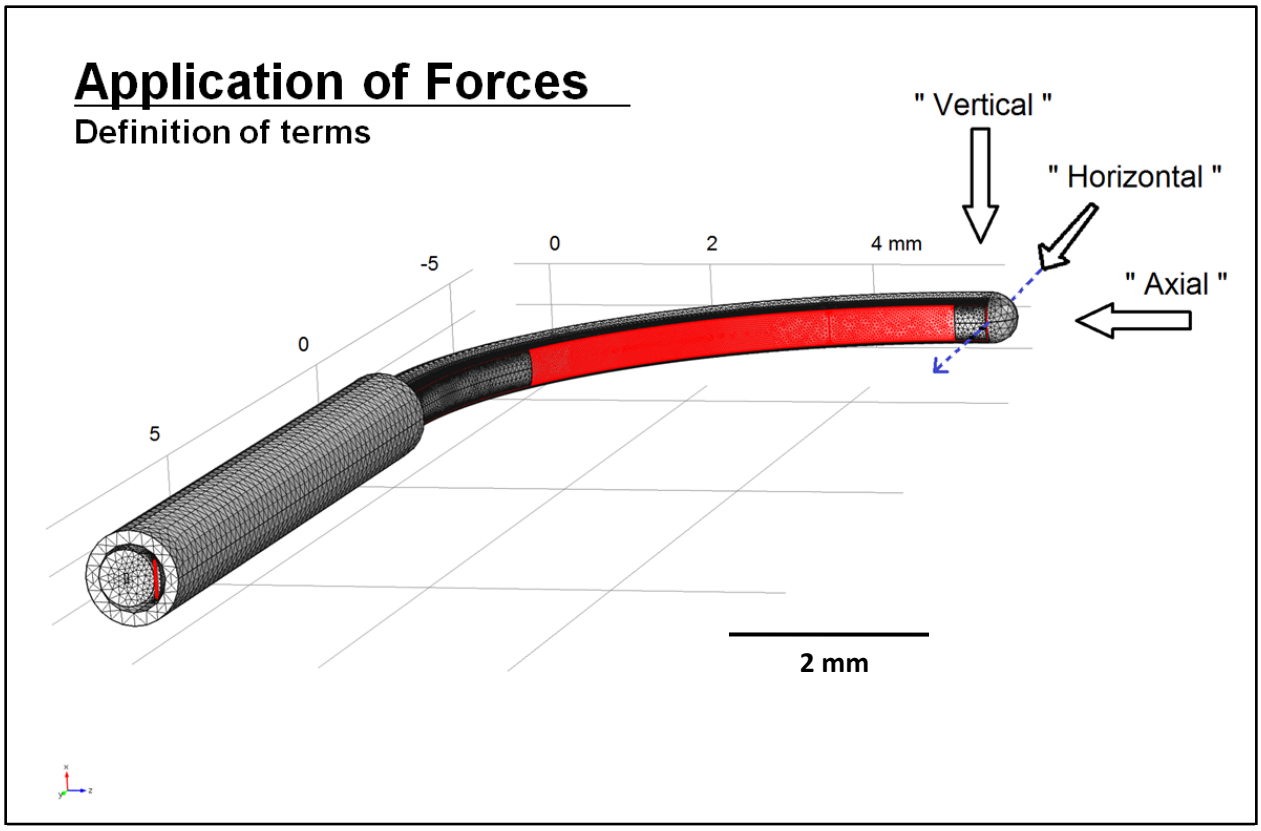

Fig. 5.2 Diagram of applied force directions. Note that the horizontal direction is normal to the TFA plane (red), and applied horizontal forces move the array towards the modiolus. A stationary cylindrical steel holder is used to anchor the assembly in a similar manner to the physical experiments.

5.1.2 Displacement Simulations to Determine Preferential Stiffness

Table 5.2 shows the results of applying forces sequentially in all three planes (as denoted in Fig. 5.2) to the tip of a 6 mm length of a given component or assembly. The results, while seemingly erratic, verify that certain components are significantly stiffer in the vertical plane. Displacement values are not directly comparable between components due to the varying applied force, but the H/V ratio normalizes this and allows us to compare the components in terms of their relative vertical versus horizontal stiffness. Varying applied forces had to be used since certain components are orders of magnitude more flexible than others in simulation and a constant force across them would have yielded displacements well beyond the physical length of certain components. However, all of the applied forces were chosen such that component maximum tip displacements in H/V tests fell within a logical range of 0 – 10mm. One result that is misleading is that the TFA, with an H/V ratio of 369, seems to be the most important factor. In vertical force simulations, the TFA stays in its prescribed plane contrary to the more realistic real-physics scenario where the larger dimension would twist into the plane of the applied force. Consider trying to bend or compress a sheet of paper in its thinnest plane – it would simply fold away from the force.

Table 5.2 Displacement values of components under various tip loads. Despite varying tip loads, the V/H ratio for a given component normalizes the displacements so that the preferential flexibility of different devices can be compared. Tip loads were chosen to result in tip displacements that fall in a range of 0-10mm. Note that for a given device we are applying a constant force in both directions and measuring the displacement, thus a component that is stiffer in the vertical direction will have a smaller vertical displacement, meaning a larger H/V displacement ratio is favorable. This is the inverse of favoring a higher V/H measured force for a constant displacement in both directions as introduced by Rebscher and used in the physical test below.

	ITD+TFA straight	ITD+TFA curved	IE+TFA straight	IE+TFA curved	ITD	IE	TFA	Pt Core
Force (mN)	20	20	0.5	20	2	0.06	0.05	5
Vertical (mm)	2.38	0.50	0.20	1.30	0.43	4.07	0.01	0.55
Horizontal (mm)	3.49	0.86	1.83	3.90	2.09	4.07	3.69	3.41
Axial (mm)	0.09	7.06	5.31	13.10	0.05	0.90	0.00460	0.00017
H/V	**1.47**	**1.72**	**9.15**	**3.00**	**4.86**	**1.00**	**369.00**	**6.20**

5.1.3 Axially Applied Forces: Resulting Displacements and Strains

As shown in Fig. 5.2 and Table 5.2, tip loads were applied axially to the various assemblies and components. One important conclusion from this segment of the modeling is that an axially applied (normal) force to the assembly tips results in horizontal as opposed to vertical flexing. This is true in both the straight and curved simulated assemblies, as shown in Figs. 5.3 and 5.4.

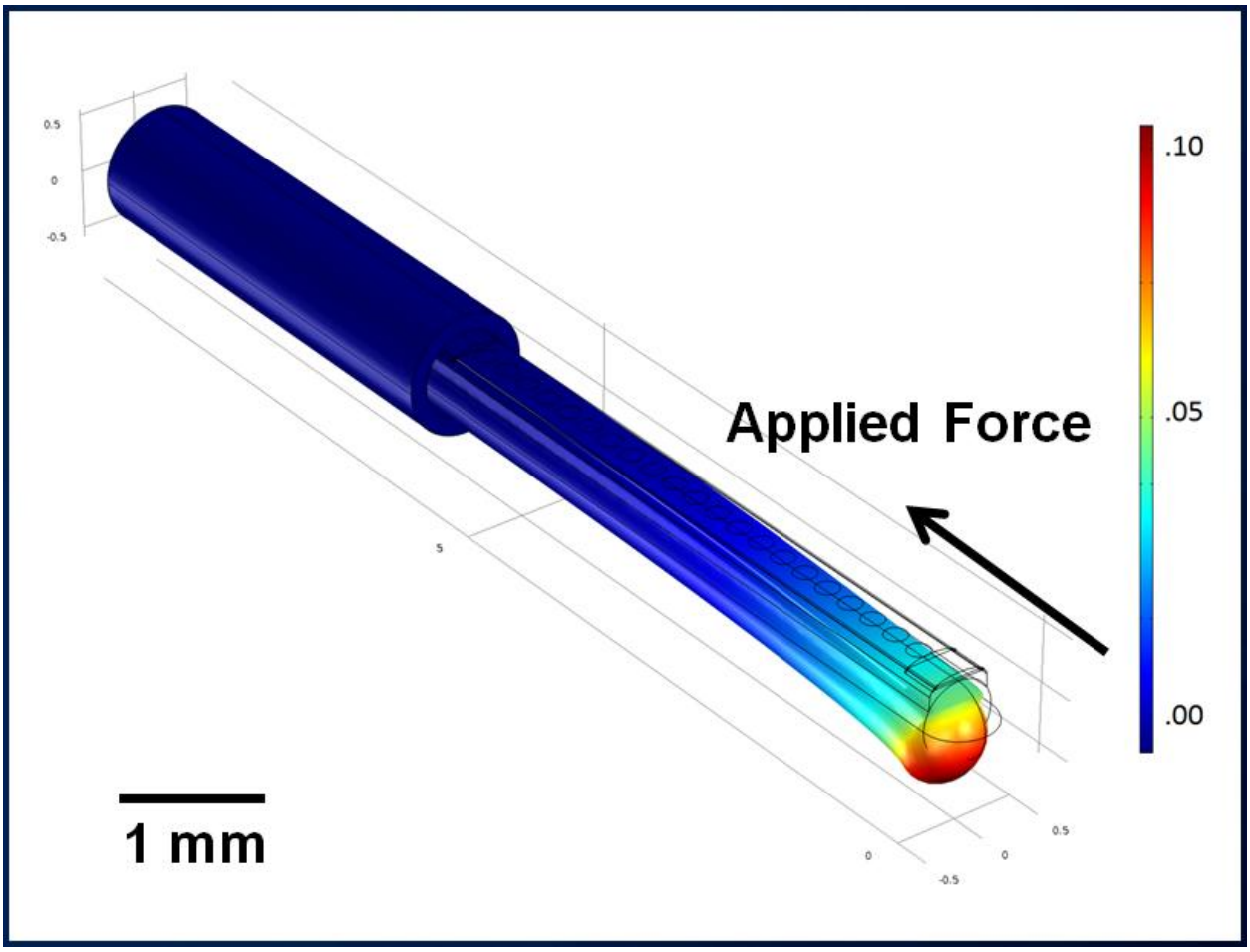

Fig. 5.3 Total displacement due to an axial 20 mN force applied to the tip of a straight TFA+ITD. The downward displacement in the figure is significant because it verifies the assembly's tendency to flex in the plane horizontal to insertion as desired. The sleeve around the basal 4 mm of the assembly serves to hold it in place while the force is applied in similar fashion to the physical testing described in the following section.

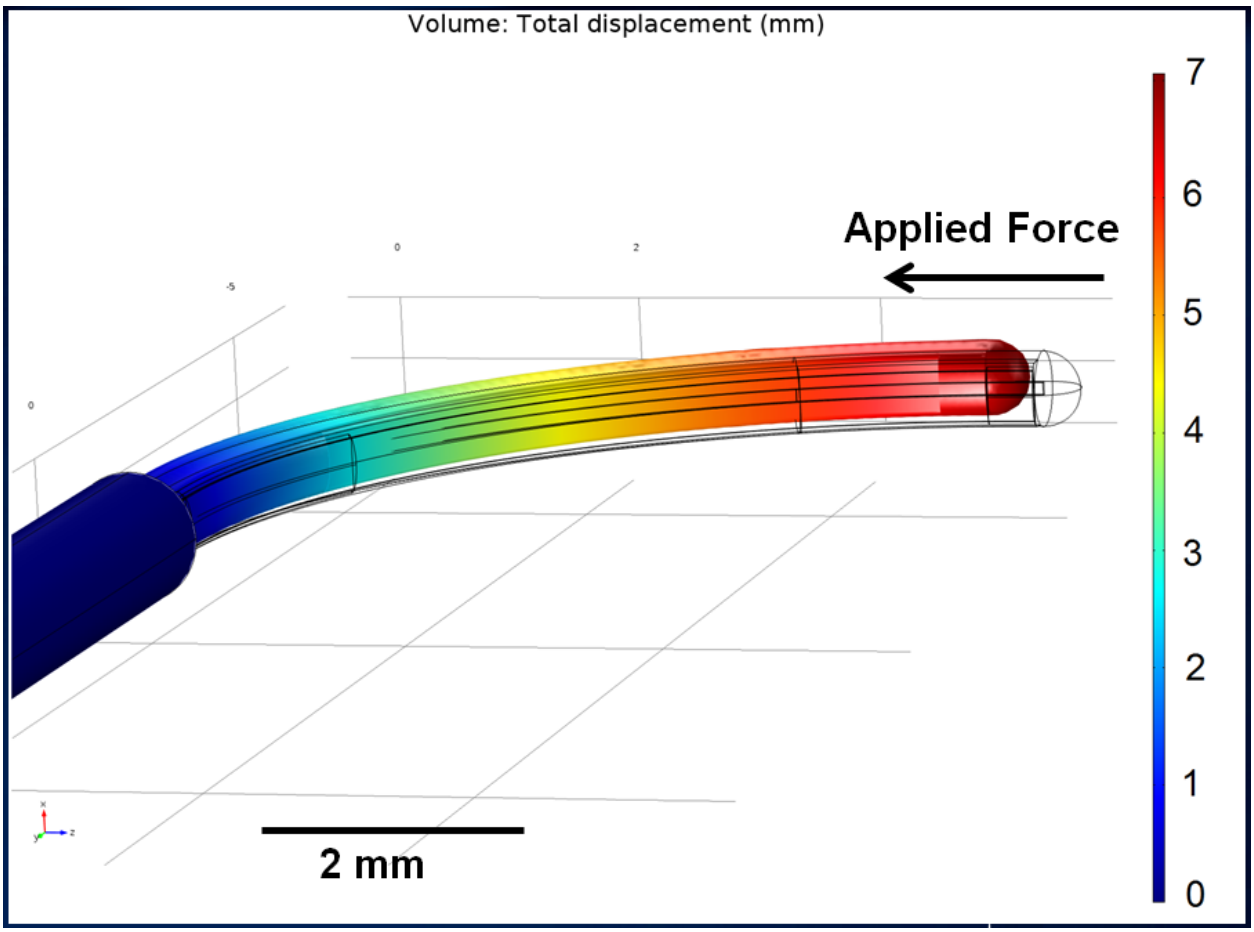

Fig. 5.4 Total displacement due to an axial 20 mN force applied to the tip of a curved TFA+ITD. Again, the nature of the displacement is significant because it verifies the assembly's tendency to flex in the plane horizontal to insertion as desired.

Another important conclusion from this segment and COMSOL modeling in general is the concentration of strain within an assembly during applied tip forces. As mentioned previously, a driving motivation for this work is the issue of TFA delamination from the IP. Fig. 5.5 below reveals that upon application of a 20 mN horizontal force (normal to the electrode plane) there is a significant shearing force between the TFA and glue layers due to a 300 X differential in material strains at the interface. Engineering Strain e, given by $e = \frac{l-L}{L}$ where l is the final length and L is the initial length along a single axis, is a relative measure of deformation versus initial shape due to an applied stress (force). Thus, the silicone materials have deformed

around 300 times as much as the TFA layer. However, when the same axial force is applied to a curved assembly the difference in strain is reduced by an order of magnitude (Fig. 5.6). This differential strain in general is an important design criterion to take into account when creating a flexible assembly to accommodate a range of positions, and means that extra steps must be taken to ensure that the layers do not come apart.

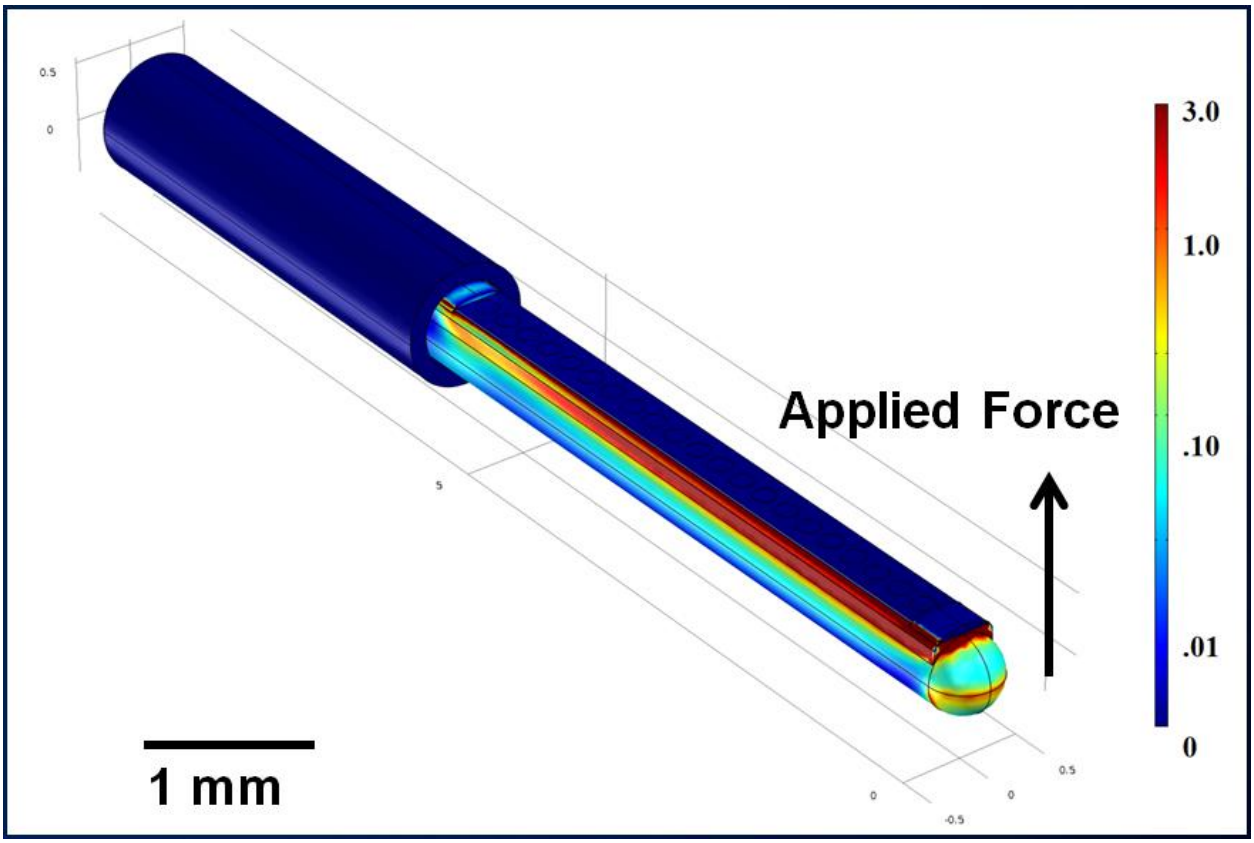

Fig. 5.5 Strain analysis of a 20 mN horizontal force applied to the tip of a straight ITD+TFA in simulation (keep in mind that "horizontal" is in reference to an electrode's positioning within the scala tympani, thus the direction normal to the electrode plane is horizontal). The color scale is normalized so that dark blue represents a strain of 0 - .02, and dark red represents a strain of 2-3. As you can see, in simulation the differential strain at the interface between the IP and the adhesive layer is two orders of magnitude indicating that there would be a significant shearing force between the layers.

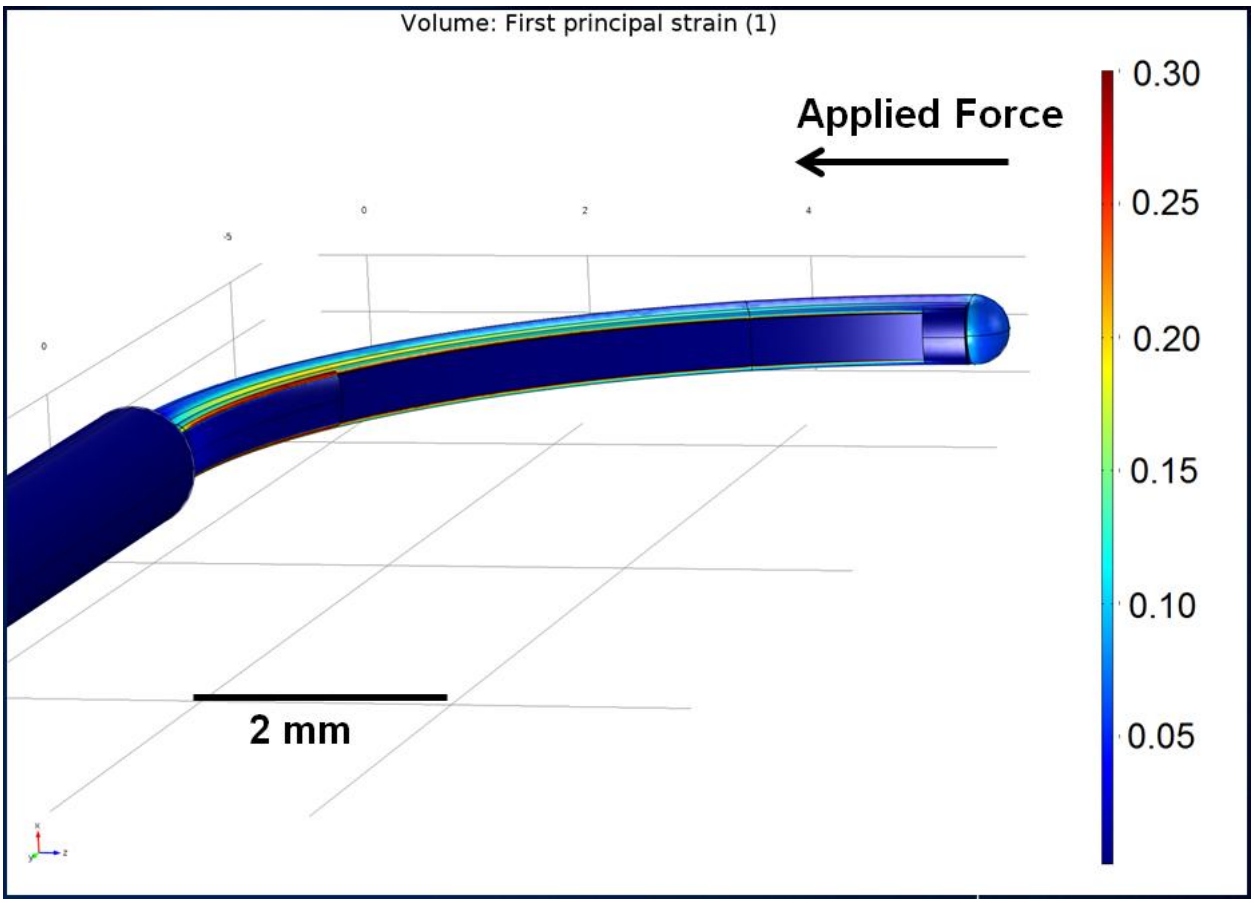

Fig. 5.6 Strain analysis of a 20 mN horizontal force applied to the tip of a curved ITD+TFA in simulation. As the color scale shows, volumetric strain has decreased by an order of magnitude in comparison to the straight assembly, thus providing motivation for pre-curving the assembling so that shearing forces between the components are minimized.

A drawback of the simulations in general is the incomparability with physical testing. The results are well out of the ranges shown in both our physical deflection tests described in the next section, as well as the Rebscher experiment off of which they are based. While great care was taken to accurately define all material properties and simulation boundary conditions, it is possible that a lack of experience with the COMSOL environment could have resulted in the differences between simulated and observed results. Some results however do appear accurate, such as the V/H flexibility ratio of ITD+TFAs which is simulated to be 1.47 and 1.72 versus measured as 1.47.

5.2 Mechanical Force Testing

In a similar manner to the previously described Rebscher procedure, a mechanical force jig was constructed to quantify the force required to deflect an array 30° 2 mm from an anchor point. This test was repeated at 2 mm intervals along the apical 10 mm of both finished assemblies and bare IP's in both the vertical and horizontal orientations. The apical 10 mm was used instead of the 6 mm used by Rebscher to be able compare flexibility in the portion of the assembly with a second adhesive layer, which begins around 6 mm. Including these measurements in the V/H force ratio calculations only changes (increases) the ratios by 3% for the IE+TFA and 4% for the ITD+TFA, thus the comparison to the Rebscher results can still be drawn. Fig. 5.7 pictures the setup used, and Table 5.3 displays the recorded measurements from testing three assemblies of each kind as well as a bare ITD and IE. The intrinsic mass of the assembly or IP tip is negligible considering 10 mm of an ITD+TFA assembly has a mass of at most 5 mg, an order of magnitude less than the least significant digit recorded in the measurements.

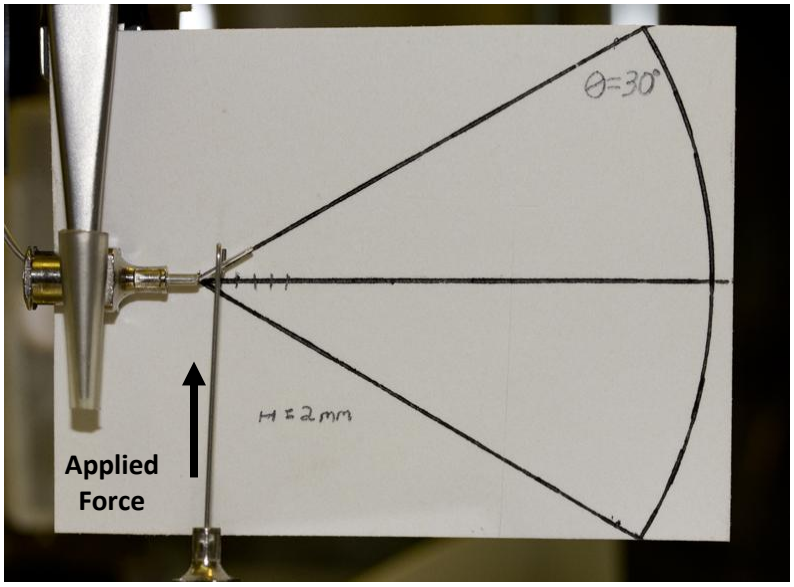

Fig. 5.7 Mechanical force rig constructed to measure deflection forces in assemblies and insertion platforms. The assembly or IP is held in place by a micromanipulator which lowers the protruding tip onto a stand that rests on an analytical balance (Sartorius CPA324S, Sartorius AG, Göttingen, Germany). The balance registers the gram-force necessary to deflect the protruding tip to an angle of 30°. This procedure is repeated at 2 mm intervals along the apical 10 mm of each component, and in both horizontal and vertical orientations.

Table 5.3 Summary of average Vertical/Horizontal force requirements for the assemblies and components. The recorded measurements for all devices, including 6 assembles and two insertion platforms tested in both orientations, can be found in Appendix A3. Notice that even though the ITD+TFA has an inner platinum core to promote horizontal deflection, the IE based assembly has a higher V/H ratio. This is because the IE assembly does not contain any components that offer significant resistance to horizontal bending, thus raising the V/H ratio. All force measurements are in grams-force

Distance	ITD	IE	ITD+TFA	IE+TFA
2 mm	1.09	0.88	2.08	1.74
4 mm	1.34	1.00	1.28	2.00
6 mm	0.98	1.00	1.23	1.67
8 mm	1.10	0.92	1.34	1.75
10 mm	1.22	1.00	1.42	1.58
Average	1.15	0.96	1.47	1.75

There are interesting trends to note in this data. First of all, both assemblies and the plain ITD are selective to deflection in the horizontal plane, which was the desired outcome. Secondly, the IE based assembly actually has a greater V/H ratio than the ITD based assembly despite the fact that the ITD has a platinum core to promote horizontal deflection and thus raise the V/H ratio. This makes sense however because the IE based assembly does not have any components that provide meaningful resistance to horizontal flexing; the only significant resistance to flexing in any direction comes from the TFA and that is in the vertical direction. The COMSOL simulations corroborate this result and also provide insight as to how dominating the platinum core is to assembly performance: it adds significant stiffness in both planes, increasing the average vertical and horizontal stiffness from .10 and .11 grams-force in the IE to 1.19 and 1.04 grams-force in the ITD. Fig. 5.8 provides a visual comparison of the V/H ratios of the various components. Note that the pure silicone IE lies directly on the line y = x (vertical stiffness = horizontal stiffness) and all other devices lie above the line in the region of higher vertical stiffness.

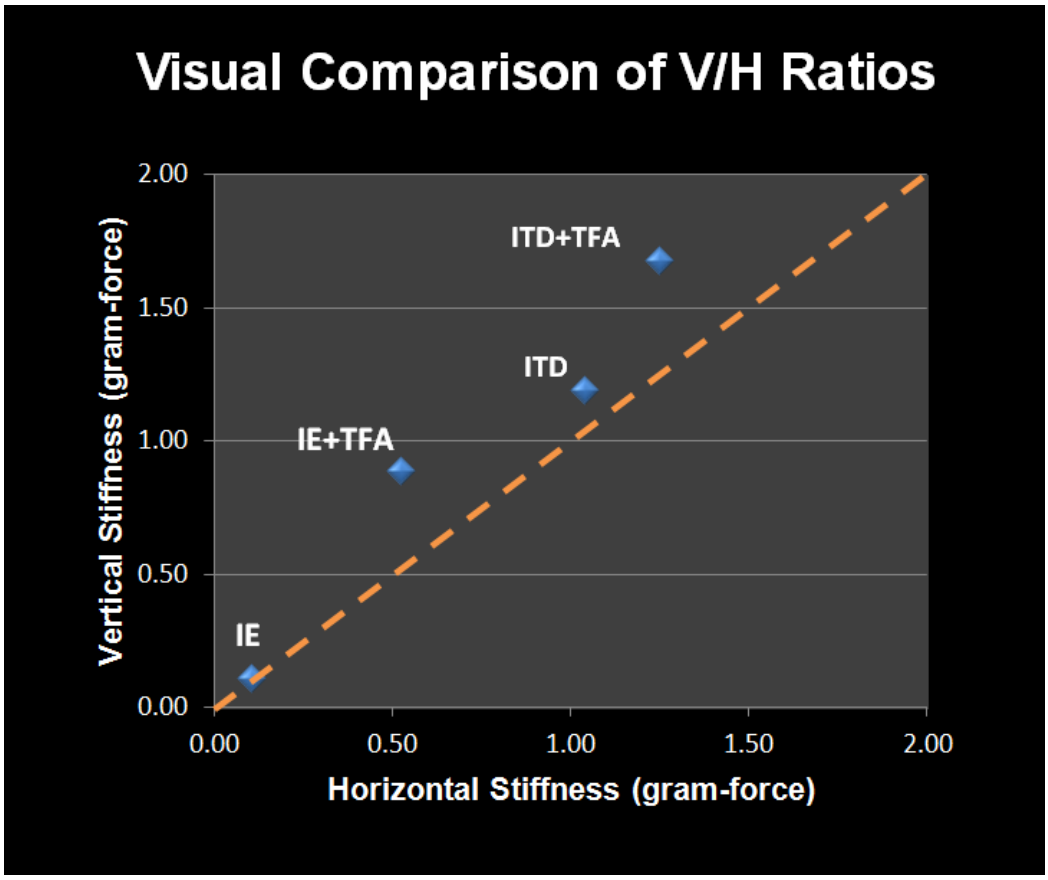

Fig. 5.8 Graphical display of average vertical versus horizontal stiffness in tested devices. The IE, made of pure silicone with no components to influence selective flexibility, lies directly on the line y = x. All other devices lie in the region of greater vertical stiffness, or increased selectivity to flex in the horizontal direction.

The results of the physical force test are well within the anticipated range of values. Rebscher, who used wire core arrays that are stiffer than our assemblies, obtained deflection forces on the order of 1-3 grams. The results confirm our suspicions that the assemblies would be more flexible than commercial options, with average forces being slightly less than Rebscher's measurements.

5.3 Electrical Impedance Testing

TFA electrodes involve extremely thin transmission lines to deliver current from the connection with higher circuitry to the electrode site on the array. This has the potential to increase site impedances, so all precautions must be taken to ensure that the assembly and insertions procedures do not adversely affect electrical performance of the arrays. Specifically, the second layer of glue must be kept off of the active sites, and array kinking due to excessive insertion forces must be avoided. To investigate this, the two assemblies with connectors from the insertion study were examined visually post-assembly to verify that the contacts were glue-free, and then they were tested to determine site impedances pre- and post-implantation. The results are listed in Table 5.5.

In order to determine site impedances a three electrode setup was connected to a Metrohm Autolab PGSTAT (Metrohm AG, Herisau, Switzerland) and submerged in a 1X (.1M) PBS solution at room temperature. The PBS solution was mixed according to Table 5.4, and the final pH and temperature were measured to be 7.4 and 22.5°C, respectively, using an Oakton® Acorn™ pH 5 Meter (Oakton Instruments, Vernon, IL). A 1 kHz, 50 mA sine wave was applied to each site individually according to previous impedance verification procedures [39], [53], [57]. Because the harvested temporal bones had been cured in formaldehyde, the bones were allowed to soak submerged in PBS for 72 hours before post-implantation measurements were obtained to allow for more natural conductances in the tissue.

The pre- and post-implantation impedance results for the two assemblies with connectors show no statistically significant changes: paired two-sample t-tests (assuming a normal distribution of impedance values) resulted in p-values of greater than .05, although one was only slightly larger and is in fact shown to be non-randomly distributed, this nullifying the t-test. Although the results were technically statistically insignificant for the other assembly tested, the large fluctuations in site impedances for some individual electrodes raise suspicions and suggest that more arrays should be tested. Overall, further testing to show consistent site

impedances is important because it would validate that the new assembly structure can be implanted without causing significant changes or structural trauma to the array that would result in a decreased ability for the electrode sites to deliver current.

Table 5.4 The following compounds were mixed in a 100 mL volumetric flask to form a 10X PBS concentration. For use, 10 mL of this was diluted to 1X (.01M) by combining 1:10 with distilled water in a beaker. Th pH and temperature of the final solution were measured to be 7.4 and 22.5° C, respectively, at the time of use.

Na2HPO4 (anhydrous) ----------	1.09 g (Alfa Aesar, lot#K15R024)
NaH2PO4 (anhydrous) ----------	0.32 g (Alfa Aesar, lot#A14U011)
NaCl ----------	9.00 g (BDH, lot#YA2031NFDI)
Distilled water ----------	100 mL

Table 5.5 Electrical Impedance testing of array sites. Array 25F8 was supplied with factory impedance data. Only data for sites 1-16 were used for 37B0, and 1-14 for 25F8 due to errors in equipment connection. The transformation of "errors" into ultra-high impedance transmissions in post-assembly testing suggests that the initial error is in the array or attached connector, and some sort of leakage current is able to develop due to the 72 hour PBS soak.

Array:	**37B0**			
Trial:	Pre-Assembly	Post-Assembly (kΩ)	Post Insertion (kΩ)	
Site				Δ
1	-	27.3	61.2	33.9
2	-	26.7	15.1	-11.6
3	-	27.7	71.3	43.6
4	-	26.8	14.0	-12.8
5	-	27.1	68.5	41.4
6	-	29.9	15.5	-14.4
7	-	28.3	124	95.7
8	-	29.0	14.3	-14.7
9	-	29.7	83.5	53.8
10	-	28.9	14.6	-14.3
11	-	20.4	38.2	17.8
12	-	22.3	13.6	-8.7
13	-	27.2	87.3	60.1
14	-	21.8	12.7	-9.1
15	-	53.2	177	123.8
16	-	28.3	12.35	-16.0
17	-	error	2140	
18	-	error	2200	

Table 5.5 Continued

19	-	error	2030	
20	-	error	2110	
21	-	25.9	14.2	-11.7
24(gnd)	-	-	4.05	
			Mean Change:	21.0
			Std Deviation:	43.3
			Variance:	1878.6
			Mean % Change:	112.7

Array:	**25F8**			
Trial:	Pre-Assembly (MΩ)	Post-Assembly (kΩ)	Post Insertion (kΩ)	
Site				Δ
1	0.05	211	165	-46.0
2	0.05	132	195	63.0
3	0.05	293	177	-116.0
4	0.05	332	164	-168.0
5	0.03	105	141	36.0
6	0.03	132	160	28.0
7	0.05	125	148	23.0
8	0.05	111	163	52.0
9	0.03	117	152	35.0
10	0.05	126	189	63.0
11	0.03	225	215	-10.0
12	0.04	130	180	50.0
13	0.04	740	171	-569.0
14	0.04	212	186	-26.0
15	0.02	1740	186	-1554.0
16	0.02	1150	188	-962.0
17	0.05	error	2300	
18	0.05	error	2180	
19	0.05	error	2050	
20	0.05	error	2210	
21	34.71	133	1680	1547.0
24(gnd)		-	170	
			Mean Change:	-91.4
			Std Deviation:	611.2
			Variance:	373551.5
			Mean % Change:	107.6

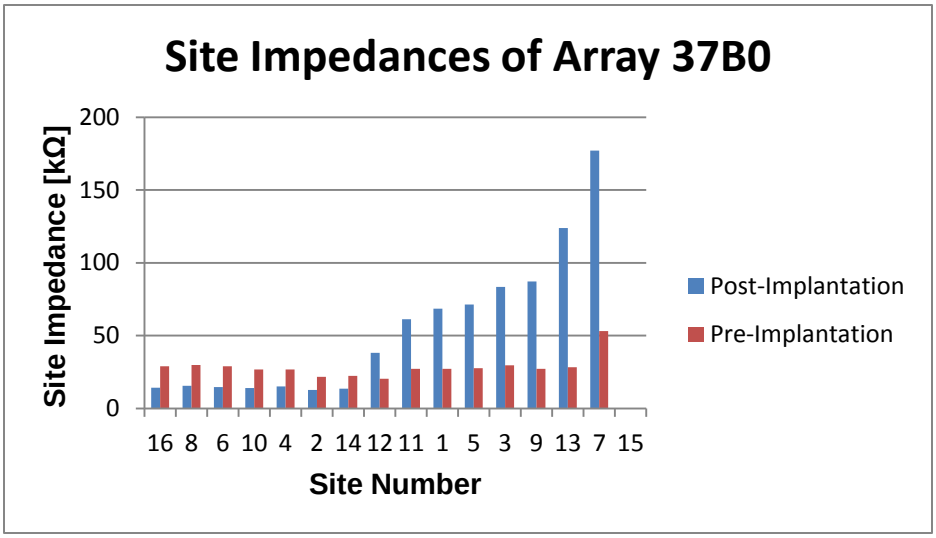

Fig. 5.9 Histogram showing pre- and post-implantation site impedances for array 37B0. The data was sorted from smallest to largest post-implantation impedance to visually reveal the bi-modal distribution of the results. You can see that all but one positively labeled site decreased in impedance, and all negative site numbers increased in impedance. This suggests a selective flaw in the array that results in non-randomly distributed data, and the fact that all even sites use one connector while all odd sites use a second connector seems like a likely explanation for the differences (refer to Fig. 4.11). The p-value assuming a random distribution for this data is .053, which hints at a non-random correlation. The seemingly bi-modal distribution in fact nullifies the ability to use a t-test, and no statistically significant conclusions can be drawn from the results**.**

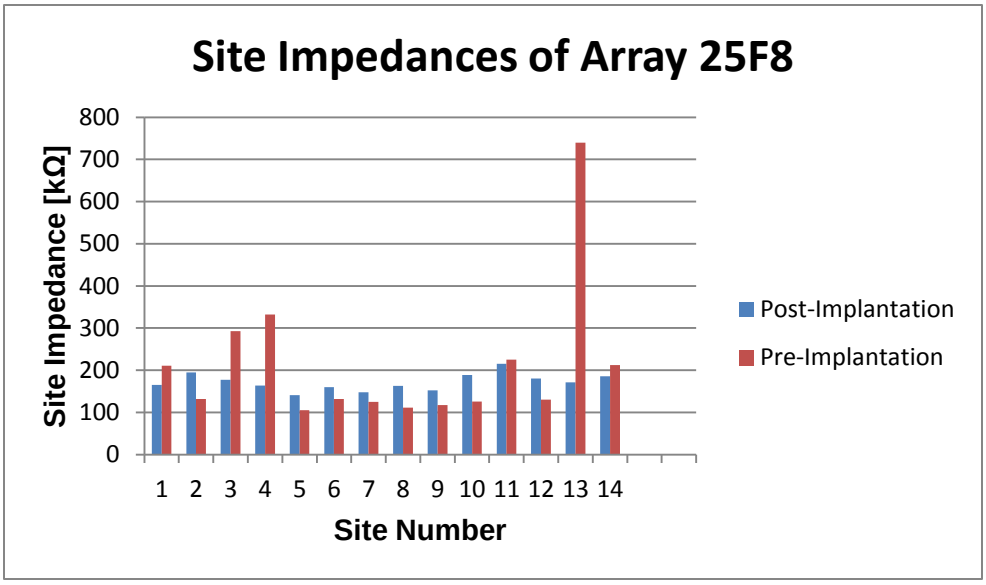

Fig. 5.10 Histogram showing pre- and post-implantation site impedances for array 25F8. This data shows a more normal distribution, and sorting similar to the previous example reveals no unique distribution. The p-value from a two-tailed t-test for this data is .365, meaning the results are statistically significant. However, the fact that two datapoints were thrown out due to assumed connection errors leaves less confidence in the results.

5.4 Cadaveric Temporal Bone Insertion Study

In order to verify the efficacy of the new assemblies and molding procedure, a cadaver study was performed on 10 temporal bones harvested from human cadavers by the Georgia Health Sciences University (Augusta, GA). This study implanted (4) assemblies composed of ITD's molded to inactive arrays, (4) composed of IE's molded to inactive arrays, and (2) assemblies that used active TFA's with connectors molded to IE's. Dr. Brian McKinnon and Dr. Jessica Van Beek-King of the GHSU supplied the temporal bones and performed the physical insertions. The temporal bones had been dried in formaldehyde after harvesting, so a medical lubricating gel was used to facilitate a smooth insertion. Of the 10 assembly insertions that were attempted, all but two successfully inserted. The two that failed, one each of an IE and ITD, delaminated at the tip due to stress during initial insertion into the cochlear first turn. This was

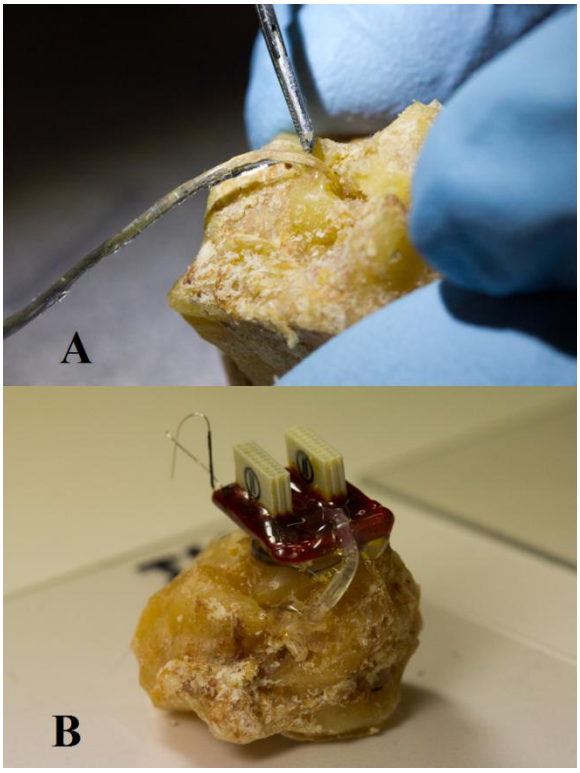

Fig. 5.11 Implantation of an IE + Array with connector. Figure A shows the curved tip of the assembly just beginning to enter the round window, and Figure B shows the fully inserted assembly where the connector is mounted to the temporal bone with hot glue.

unexpected due to the improvements that had been made since the first study, and suggests that further strengthening of the molded assembly is necessary. Fig. 5.11 shows images taken during the insertion of an assembly with a connector. View A shows the assembly as it is just beginning to be inserted into the round window of the cochlea, and you can see that the tip of the assembly has a natural curvature due to the molding process. This curvature added some degree of difficulty to the initial insertion and led to a tip delamination as the tip interacted with the rough outer surface of the dried temporal bone. Fig. 5.11 B then shows the fully inserted assembly, and the connector has been hot-glued to the temporal bone to ensure that the assembly doesn't pull out during transportation and electrical impedance testing. Further histological and micro-CT evaluation of the insertions by colleagues at Emory University Hospital is pending.

CHAPTER 6: CONCLUSIONS

6.1 Summary of Results

The preceding chapters introduced the chronic disability of hearing loss, examining the physiology of the human auditory system and the proposed mechanisms by which humans lose their ability to hear. Trauma to hair cells of the inner ear decreases our ability to transduce neural impulses from the mechanical vibrations of natural auditory events. Hearing aids can often overcome a significant degree of hearing loss by amplifying environmental sounds, however when extreme loss or total deafness occurs there is no longer sufficient functionality in the natural transduction mechanism. Cochlear implants attempt to overcome this issue by bypassing the hair cells completely and directly targeting the auditory neurons that they connect to in the spiral ganglion of the cochlea. Cochlear implants are the most widely available and successful neural implant in medicine, although the composition of the electrode array has remained relatively unchanged throughout its more recent history.

This work has shown that a new method for creating electrodes based on thin-film array technology offers an opportunity to expand on the density and total number of electrodes available in an implant. Polyimide based TFA's have been previously shown to be biocompatible and bio-stable in long term implantable devices, but they have yet to be used in a clinical or commercial cochlear implant. Polyimide TFA's present unique mechanical challenges to surgical insertion due to their small profile and extreme flexibility. In order to provide a more viable solution for implantation, this work has described a novel method for combining the TFA's with silicone based surgical backings that allows the electrodes to be successfully inserted to standard insertion depths in the cochlea. The inherent properties of these assemblies make them more flexible in the plane that is horizontal to the plane of insertion, thus decreasing the risk of surgical trauma from vertical movement that could damage the fragile membranes of the

cochlear duct. The assemblies are also molded in a slightly curved position for two reasons: The first is to decrease total shearing forces experienced between the array and insertion platform during surgical insertion and conformation to the spiral nature of the cochlea, and the second is to promote perimodiolar placement of the array in the cochlea to increase electrode selectivity. Finally, the mechanical and functionality of these assemblies was verified through finite element modeling simulations in COMSOL, stiffness quantification with a mechanical force rig, and a physical insertion study into human cadaveric temporal bones.

6.2 Future Directions

While these assembled arrays offer promising improvements on previous TFA based electrode work, there are still significant obstacles to overcome. As highlighted by COMSOL modeling, the extreme difference in the material nature of the IP's and TFA's generates a significant shearing force at the adhesive boundary. This means that any intentional or unintentional bending and deflection upon surgical insertion or final conformation to the physiology of the cochlea presents an increasing chance of delamination. Molding the assemblies in an intermediate curvature between that required for perimodiolar placement in the cochlea and uniformly straight for ease of surgical insertion somewhat mitigates these risks. However, feedback from the surgeons during the temporal bone study suggests that even this intermediate curvature may present too much difficulty during insertion. One answer to this would be the use of a surgical stylet or external sheath to straighten the electrode assembly during insertion as discussed previously in reference to currently available clinical and commercial technologies for wire-based electrodes. Shearing forces would more than likely still be a significant factor during the straightening of a pre-curved array however. An ideal insertion platform would anchor the TFA at the tip and would allow it to slide freely elsewhere while still managing to hold it in place and guide it to a perimodiolar placement, suggesting that the ultimate solution would employ an IP molded to fit with the specific dimensions of the TFA's.

APPENDIX A1

MATLAB code for the Cochlear Implant Simulator presented in section 3.3:

```
function varargout = Audio_Filterbanding_stable_with_envelope_0324(varargin)
% AUDIO_FILTERBANDING M-file for Audio_Filterbanding.fig
%      FC=[550 650 700 850 2000 2500 4200 4700]
%      AUDIO_FILTERBANDING, by itself, creates a new AUDIO_FILTERBANDING or
raises the existing
%      singleton*.
%
%      H = AUDIO_FILTERBANDING returns the handle to a new
AUDIO_FILTERBANDING or the handle to
%      the existing singleton*.
%
%      AUDIO_FILTERBANDING('CALLBACK',hObject,eventData,handles,...) calls
the local
%      function named CALLBACK in AUDIO_FILTERBANDING.M with the given input
arguments.
%
%      AUDIO_FILTERBANDING('Property','Value',...) creates a new
AUDIO_FILTERBANDING or raises the
%      existing singleton*.  Starting from the left, property value pairs are
%      applied to the GUI before Audio_Filterbanding_OpeningFcn gets called.
An
%      unrecognized property name or invalid value makes property application
%      stop.  All inputs are passed to Audio_Filterbanding_OpeningFcn via
varargin.
%
%      *See GUI Options on GUIDE's Tools menu.  Choose "GUI allows only one
%      instance to run (singleton)".
%
% See also: GUIDE, GUIDATA, GUIHANDLES

% Edit the above text to modify the response to help Audio_Filterbanding

% Last Modified by GUIDE v2.5 26-Apr-2011 00:04:20

% Begin initialization code - DO NOT EDIT


gui_Singleton = 1;
gui_State = struct('gui_Name',       mfilename, ...
                   'gui_Singleton',  gui_Singleton, ...
                   'gui_OpeningFcn', @Audio_Filterbanding_OpeningFcn, ...
                   'gui_OutputFcn',  @Audio_Filterbanding_OutputFcn, ...
                   'gui_LayoutFcn',  [] , ...
                   'gui_Callback',   []);
if nargin && ischar(varargin{1})
    gui_State.gui_Callback = str2func(varargin{1});
```

```
end

if nargout
    [varargout{1:nargout}] = gui_mainfcn(gui_State, varargin{:});
else
    gui_mainfcn(gui_State, varargin{:});
end
% End initialization code - DO NOT EDIT
end


% --- Executes just before Audio_Filterbanding is made visible.
function Audio_Filterbanding_OpeningFcn(hObject, eventdata, handles,
varargin)
% This function has no output args, see OutputFcn.
% hObject    handle to figure
% eventdata  reserved - to be defined in a future version of MATLAB
% handles    structure with handles and user data (see GUIDATA)
% varargin   command line arguments to Audio_Filterbanding (see VARARGIN)

% Choose default command line output for Audio_Filterbanding
handles.output = hObject;

% Update handles structure
guidata(hObject, handles);

% UIWAIT makes Audio_Filterbanding wait for user response (see UIRESUME)
% uiwait(handles.figure1);
end

% --- Outputs from this function are returned to the command line.
function varargout = Audio_Filterbanding_OutputFcn(hObject, eventdata,
handles)
% varargout  cell array for returning output args (see VARARGOUT);
% hObject    handle to figure
% eventdata  reserved - to be defined in a future version of MATLAB
% handles    structure with handles and user data (see GUIDATA)

% Get default command line output from handles structure
varargout{1} = handles.output;
end

% --- Executes on button press in Select_Source_Audio.
function Select_Source_Audio_Callback(hObject, eventdata, handles)
% hObject    handle to Select_Source_Audio (see GCBO)
% eventdata  reserved - to be defined in a future version of MATLAB
% handles    structure with handles and user data (see GUIDATA)

global audio_enveloped_out audio_banded_out audio_in Fs Ymax checkbox_ENV;
clear audio_enveloped_out audio_banded_out
checkbox_ENV=0;

%clear axes
axes(handles.axes2)
cla(handles.axes2,'reset')
```

```
Ymax_Callback(handles.Ymax,eventdata,handles)

[audio_file_in, PATHNAME, FILTERINDEX] = uigetfile('*.wav','Select Audio
File');
[audio_in,Fs,NBITS]=wavread(audio_file_in);
%Force audio file to mono-----------------------------------------------------
size_audio_in=size(audio_in);
if size_audio_in(:,2)== 1
    audio_in=audio_in;
elseif size_audio_in(:,2)==2
    audio_in=(audio_in(:,1)+audio_in(:,2))/2;
end
%---plot input power spectrum
x=audio_in;
x = x(:);
L = 2^ceil(log2(length(x)));
%--
   Lx = length(x);
   HammW = 0.54 - 0.46*cos(2*pi*(0:Lx-1)'/(Lx-1));
%--
XX = abs(fft(HammW.*x,L))/length(x)*3.86;
XX = XX(1:L/2);
ww = [0:L/2-1]/L*Fs;

axes(handles.axes2)
semilogx(ww,XX),axis([10 20000 0 Ymax]);
grid on;
zoom on;
xlabel('Frequency in Hz');
ylabel('Approximate Amplitude');

end

% --- Executes on selection change in set_channels.
function set_channels_Callback(hObject, eventdata, handles)
% hObject    handle to set_channels (see GCBO)
% eventdata  reserved - to be defined in a future version of MATLAB
% handles    structure with handles and user data (see GUIDATA)

% Hints: contents = cellstr(get(hObject,'String')) returns set_channels
contents as cell array
%        contents{get(hObject,'Value')} returns selected item from
set_channels
global n_bands Fs;
n_bands=get(handles.set_channels,'Value')-1;
end

% --- Executes during object creation, after setting all properties.
function set_channels_CreateFcn(hObject, eventdata, handles)
% hObject    handle to set_channels (see GCBO)
% eventdata  reserved - to be defined in a future version of MATLAB
% handles    empty - handles not created until after all CreateFcns called

% Hint: popupmenu controls usually have a white background on Windows.
```

```
%       See ISPC and COMPUTER.
if ispc && isequal(get(hObject,'BackgroundColor'),
get(0,'defaultUicontrolBackgroundColor'))
    set(hObject,'BackgroundColor','white');
end
end


% --- Executes on button press in audio_play.
function audio_play_Callback(hObject, eventdata, handles)
% hObject    handle to audio_play (see GCBO)
% eventdata  reserved - to be defined in a future version of MATLAB
% handles    structure with handles and user data (see GUIDATA)
global audio_in Fs p;
p=audioplayer(audio_in,Fs);
play(p)
end

% --- Executes on button press in audio_stop.
function audio_stop_Callback(hObject, eventdata, handles)
% hObject    handle to audio_stop (see GCBO)
% eventdata  reserved - to be defined in a future version of MATLAB
% handles    structure with handles and user data (see GUIDATA)
global p;
stop(p)
end



function Ymax_Callback(hObject, eventdata, handles)
% hObject    handle to Ymax (see GCBO)
% eventdata  reserved - to be defined in a future version of MATLAB
% handles    structure with handles and user data (see GUIDATA)

% Hints: get(hObject,'String') returns contents of Ymax as text
%        str2double(get(hObject,'String')) returns contents of Ymax as a
%        double
global Ymax audio_in Fs;
input = str2num(get(hObject,'String'));

%checks to see if input is empty. if so, default input1_editText to zero
if (isempty(input))
     set(hObject,'String','.05')
end
guidata(hObject, handles);
Ymax = str2num(get(handles.Ymax,'String'));

%---Re-plot input power spectrum------------
x=audio_in;
x = x(:);
L = 2^ceil(log2(length(x)));
%--
   Lx = length(x);
   HammW = 0.54 - 0.46*cos(2*pi*(0:Lx-1)'/(Lx-1));
%--
```

```
XX = abs(fft(HammW.*x,L))/length(x)*3.86;
XX = XX(1:L/2);
ww = [0:L/2-1]/L*Fs;

axes(handles.axes2)
semilogx(ww,XX),axis([10 20000 0 Ymax]);
grid on;
zoom on;
xlabel('Frequency in Hz');
ylabel('Approximate Amplitude');
end

% --- Executes during object creation, after setting all properties.
function Ymax_CreateFcn(hObject, eventdata, handles)
% hObject    handle to Ymax (see GCBO)
% eventdata  reserved - to be defined in a future version of MATLAB
% handles    empty - handles not created until after all CreateFcns called

% Hint: edit controls usually have a white background on Windows.
%       See ISPC and COMPUTER.
if ispc && isequal(get(hObject,'BackgroundColor'),
get(0,'defaultUicontrolBackgroundColor'))
    set(hObject,'BackgroundColor','white');
end
end



% --- Executes on button press in initiate_filter.
function initiate_filter_Callback(hObject, eventdata, handles)
% hObject    handle to initiate_filter (see GCBO)
% eventdata  reserved - to be defined in a fsuture version of MATLAB
% handles    structure with handles and user data (see GUIDATA)
global checkbox_FC audio_in Fs n_bands window_active audio_banded_out
audio_enveloped_out filter_order F_center window_active_number
channel_sim_sum;
F_center=zeros(1,n_bands);

Fsn=Fs/2;
cla(handles.axes4)
%---create successive bands----
audio_banded_out=zeros(length(audio_in),n_bands);
audio_enveloped_out=zeros(length(audio_in),n_bands);
save('aeo.mat',audio_enveloped_out)
N=filter_order;


%linear band spacing-------------
% for i=0:n_bands-1
%     a=(10^((i/n_bands)*4))*Fsn;
%     b=(10^((i+1)/n_bands)*4)*Fsn;
%     if i==0
%         Fc1 = 50;   % First Cutoff Frequency
%         Fc2 = b;  % Second Cutoff Frequency
%     elseif i==n_bands-1
%         Fc1 = a;   % First Cutoff Frequency
```

```
%         Fc2 = Fsn-100;  % Second Cutoff Frequency
%     else
%         Fc1 = a;    % First Cutoff Frequency
%         Fc2 = b;  % Second Cutoff Frequency
%     end


%logarithmic band spacing---------------
%N_bands=n_bands+1;
a=log10(200);
b=(log10(6000)-a)/(n_bands);
%FC=[500 550 560 570 1950 2150 4200 4700];

if checkbox_FC==1
    FC=evalin('base','FC');
end

for i=1:n_bands
    if checkbox_FC ==1
        Fc1=FC(1,(2*i)-1);
        Fc2=FC(1,2*i);
    else
        Fc1=10^(a+b*(i-1));
        Fc2=10^(a+b*i);
    end
    F_center(1,i)=(Fc1+Fc2)/2;

    if window_active_number==2
        % Construct an FDESIGN object and call its BUTTER method.
        h  = fdesign.bandpass('N,F3dB1,F3dB2', N, Fc1, Fc2, Fs);
    elseif window_active_number==3
        % Construct an FDESIGN object and call its CHEBY1 method.
        h  = fdesign.bandpass('N,Fp1,Fp2,Ap', N, Fc1, Fc2, 1, Fs);
    elseif window_active_number==4
        % Construct an FDESIGN object and call its CHEBY2 method.
        h  = fdesign.bandpass('N,Fst1,Fst2,Ast', N, Fc1, Fc2, 60, Fs);
    end
    Hd = design(h, window_active);

    [H,W]=freqz(Hd);
    fhat=(W*Fs)/(2*pi);
    %---plot-------------------------------------------------
    hold on
    axes(handles.axes4)

plot(fhat,20*log10(abs(H))),grid,xlabel('Frequency'),ylabel('Gain(dB)'),title
('Filter Response','FontWeight','bold'),axis([0 6500 -100 10]);

    %---filter audio to output files, do envelope detection----------------
    audio_banded_out(:,i)=filter(Hd,audio_in)
%     audio_enveloped_out=audio_banded_out(:,i+1)


    [B,A]=butter(2,0.004);
```

```
    audio_enveloped_out(:,i)=filter(B,A,abs(audio_banded_out(:,i)))


end
plot(F_center,0,'x')
hold off

% Reconstruct Audio Simulation
[rr,cc]=size(audio_enveloped_out);
tt=0:1/Fs:(rr-1)/Fs;
tt=tt';
channel_sim=ones(rr,cc);
% create a pure sinusoid at the channel center frequency, and multiply it
%   with the channel envelope
for i = 1:cc
    channel_sim(:,i)=audio_enveloped_out(:,i).*sin(2*pi*F_center(1,i)*tt);
end
%sum the newly created sinusoids into a single column
channel_sim_sum=zeros(rr,1);
for i=1:cc
    channel_sim_sum=channel_sim_sum+channel_sim(:,i);
end

end



% --- Executes on selection change in set_window.
function set_window_Callback(hObject, eventdata, handles)
% hObject    handle to set_window (see GCBO)
% eventdata  reserved - to be defined in a future version of MATLAB
% handles    structure with handles and user data (see GUIDATA)

% Hints: contents = cellstr(get(hObject,'String')) returns set_window
contents as cell array
%        contents{get(hObject,'Value')} returns selected item from set_window
global window_active window_active_number;
window_active_number=get(handles.set_window,'Value');

if window_active_number==2
    window_active=('butter');
elseif window_active_number==3
    window_active=('cheby1');
elseif window_active_number==4
    window_active=('cheby2');
end

end

% --- Executes during object creation, after setting all properties.
function set_window_CreateFcn(hObject, eventdata, handles)
% hObject    handle to set_window (see GCBO)
% eventdata  reserved - to be defined in a future version of MATLAB
% handles    empty - handles not created until after all CreateFcns called
```

```
% Hint: popupmenu controls usually have a white background on Windows.
%       See ISPC and COMPUTER.
if ispc && isequal(get(hObject,'BackgroundColor'),
get(0,'defaultUicontrolBackgroundColor'))
    set(hObject,'BackgroundColor','white');
end
end


% --- Executes on selection change in output_channel_select.
function output_channel_select_Callback(hObject, eventdata, handles)
% hObject    handle to output_channel_select (see GCBO)
% eventdata  reserved - to be defined in a future version of MATLAB
% handles    structure with handles and user data (see GUIDATA)

% Hints: contents = cellstr(get(hObject,'String')) returns
output_channel_select contents as cell array
%        contents{get(hObject,'Value')} returns selected item from
output_channel_select
global channel_out audio_banded_out Fs active_channel_data Ymaxout F_center
checkbox_ENV audio_enveloped_out channel_sim_sum;

Ymaxout_Callback(handles.Ymaxout,eventdata,handles)

channel_out=get(handles.output_channel_select,'Value')-1;



if channel_out >=1 && channel_out <=16 && checkbox_ENV==0
    active_channel_data=audio_banded_out(:,channel_out);
elseif channel_out >=1 && channel_out <=16 && checkbox_ENV==1
    active_channel_data=audio_enveloped_out(:,channel_out);
elseif channel_out == 17
    active_channel_data=channel_sim_sum;
end

if channel_out >=1
    x=active_channel_data;
    x = x(:);
    L = 2^ceil(log2(length(x)));
    %--
       Lx = length(x);
       HammW = 0.54 - 0.46*cos(2*pi*(0:Lx-1)'/(Lx-1));
    %--
    XX = abs(fft(HammW.*x,L))/length(x)*3.86;
    XX = XX(1:L/2);
    ww = [0:L/2-1]/L*Fs;
end

if  channel_out >=1 && checkbox_ENV==0
    axes(handles.axes3)
    cla(handles.axes3,'reset')
    semilogx(ww,XX),axis([10 20000 0 Ymaxout]);
    grid on;
```

```
    zoom on;
    xlabel('Frequency in Hz');
    ylabel('Approximate Amplitude');

    %print fcenter
    if channel_out <= 16
        set(handles.Fc_out,'String',F_center(1,channel_out));
    end
elseif channel_out >=1 && channel_out <=16 && checkbox_ENV == 1
    axes(handles.axes3)
    cla(handles.axes3,'reset')
    plot(audio_banded_out(:,channel_out)),axis auto
    hold on
    plot(audio_enveloped_out(:,channel_out), 'r', 'linewidth', 2)
elseif channel_out ==17 && checkbox_ENV == 1
   axes(handles.axes3)
   cla(handles.axes3,'reset')
   plot(audio_banded_out),axis auto
   hold on
   plot(audio_enveloped_out, 'r', 'linewidth', 2)
end
end

% --- Executes during object creation, after setting all properties.
function output_channel_select_CreateFcn(hObject, eventdata, handles)
% hObject    handle to output_channel_select (see GCBO)
% eventdata  reserved - to be defined in a future version of MATLAB
% handles    empty - handles not created until after all CreateFcns called

% Hint: popupmenu controls usually have a white background on Windows.
%       See ISPC and COMPUTER.
if ispc && isequal(get(hObject,'BackgroundColor'),
get(0,'defaultUicontrolBackgroundColor'))
    set(hObject,'BackgroundColor','white');
end
end

function Ymaxout_Callback(hObject, eventdata, handles)
% hObject    handle to Ymaxout (see GCBO)
% eventdata  reserved - to be defined in a future version of MATLAB
% handles    structure with handles and user data (see GUIDATA)

% Hints: get(hObject,'String') returns contents of Ymaxout as text
%        str2double(get(hObject,'String')) returns contents of Ymaxout as a
double
global Ymaxout audio_in Fs active_channel_data;
input = str2num(get(hObject,'String'));

%checks to see if input is empty. if so, default input1_editText to zero
if (isempty(input))
     set(hObject,'String','.05')
end
guidata(hObject, handles);
Ymaxout = str2num(get(handles.Ymaxout,'String'));
```

```
%---Re-plot input power spectrum------------
x=active_channel_data;
x = x(:);
L = 2^ceil(log2(length(x)));
%--
   Lx = length(x);
   HammW = 0.54 - 0.46*cos(2*pi*(0:Lx-1)'/(Lx-1));
%--
XX = abs(fft(HammW.*x,L))/length(x)*3.86;
XX = XX(1:L/2);
ww = [0:L/2-1]/L*Fs;

axes(handles.axes3)
semilogx(ww,XX),axis([10 6500 0 Ymaxout]);
grid on;
zoom on;
xlabel('Frequency in Hz');
ylabel('Approximate Amplitude');
end

% --- Executes during object creation, after setting all properties.
function Ymaxout_CreateFcn(hObject, eventdata, handles)
% hObject    handle to Ymaxout (see GCBO)
% eventdata  reserved - to be defined in a future version of MATLAB
% handles    empty - handles not created until after all CreateFcns called

% Hint: edit controls usually have a white background on Windows.
%       See ISPC and COMPUTER.
if ispc && isequal(get(hObject,'BackgroundColor'),
get(0,'defaultUicontrolBackgroundColor'))
    set(hObject,'BackgroundColor','white');
end
end

function set_filter_order_Callback(hObject, eventdata, handles)
% hObject    handle to set_filter_order (see GCBO)
% eventdata  reserved - to be defined in a future version of MATLAB
% handles    structure with handles and user data (see GUIDATA)

% Hints: get(hObject,'String') returns contents of set_filter_order as text
%        str2double(get(hObject,'String')) returns contents of
set_filter_order as a double
global filter_order;
input_order = str2num(get(hObject,'String'));

%checks to see if input is empty. if so, default input1_editText to zero
if (isempty(input_order))
     set(hObject,'String','20')
end
guidata(hObject, handles);
filter_order = str2num(get(handles.set_filter_order,'String'));

end

% --- Executes during object creation, after setting all properties.
```

```
function set_filter_order_CreateFcn(hObject, eventdata, handles)
% hObject    handle to set_filter_order (see GCBO)
% eventdata  reserved - to be defined in a future version of MATLAB
% handles    empty - handles not created until after all CreateFcns called

% Hint: edit controls usually have a white background on Windows.
%       See ISPC and COMPUTER.
if ispc && isequal(get(hObject,'BackgroundColor'),
get(0,'defaultUicontrolBackgroundColor'))
    set(hObject,'BackgroundColor','white');
end
end

% --- Executes on button press in play_out.
function play_out_Callback(hObject, eventdata, handles)
% hObject    handle to play_out (see GCBO)
% eventdata  reserved - to be defined in a future version of MATLAB
% handles    structure with handles and user data (see GUIDATA)
global active_channel_data Fs pp;
pp=audioplayer(active_channel_data,Fs);
play(pp)
end

% --- Executes on button press in stop_out.
function stop_out_Callback(hObject, eventdata, handles)
% hObject    handle to stop_out (see GCBO)
% eventdata  reserved - to be defined in a future version of MATLAB
% handles    structure with handles and user data (see GUIDATA)
global pp;
stop(pp)
end

% --- Executes on button press in checkbox1.
function checkbox1_Callback(hObject, eventdata, handles)
% hObject    handle to checkbox1 (see GCBO)
% eventdata  reserved - to be defined in a future version of MATLAB
% handles    structure with handles and user data (see GUIDATA)
% Hint: get(hObject,'Value') returns toggle state of checkbox1
global checkbox_FC;
checkbox_FC=get(hObject,'Value');
end
% --- Executes on button press in checkbox2.
function checkbox2_Callback(hObject, eventdata, handles)
% hObject    handle to checkbox2 (see GCBO)
% eventdata  reserved - to be defined in a future version of MATLAB
% handles    structure with handles and user data (see GUIDATA)
% Hint: get(hObject,'Value') returns toggle state of checkbox2
global checkbox_ENV;
checkbox_ENV=get(hObject,'Value');
end

% This is the pushbutton to start the stimulation which interfaces with the
% Arduino microcontroller.s
% --- Executes on button press in pushbutton25.
function pushbutton25_Callback(hObject, eventdata, handles)
% hObject    handle to pushbutton25 (see GCBO)
```

```
% eventdata  reserved - to be defined in a future version of MATLAB
% handles    structure with handles and user data (see GUIDATA)
% Set scale to 1600, length is 38sec
global small_audio_enveloped_out audio_enveloped_out downsample_input
audio_length audio_in Fs p
%Downsample the audio
small_audio_enveloped_out=downsample(audio_enveloped_out,downsample_input);
[total_number_of_samples
number_of_electrodes]=size(small_audio_enveloped_out)

%Normalize the small_audio_enveloped_out input
%normalized_small_audio_enveloped_out=small_audio_enveloped_out/max(max(small
_audio_enveloped_out));
%display(max(max(normalized_small_audio_enveloped_out)))
%display(min(min(normalized_small_audio_enveloped_out)))

mean_small_audio_enveloped_out=mean(mean((small_audio_enveloped_out)));
binary_small_audio_enveloped_out=
(small_audio_enveloped_out>mean_small_audio_enveloped_out);
delete(instrfind({'Port'},{'COM3'}));    % Close the serial port
pause(.5)
a=arduino('COM3');                        % Open serial port for Arudino
pause(.5)
a.pinMode(2,'output');
a.pinMode(3,'output');
a.pinMode(4,'output');
a.pinMode(5,'output');
binary_small_audio_enveloped_out=double(binary_small_audio_enveloped_out);
%Timing offset to compensate for time to run code.
%tt=.0210532 %for song, 1600 downsampling, 38 second clip;
tt=.02889; %For rugs sound, 1300 downsampling, 13 second long clip

delay=audio_length/total_number_of_samples-tt

p=audioplayer(audio_in,Fs);
play(p)
for i=1:total_number_of_samples
    a.digitalWrite(2,binary_small_audio_enveloped_out(i,1));
    a.digitalWrite(3,binary_small_audio_enveloped_out(i,2));
    a.digitalWrite(4,binary_small_audio_enveloped_out(i,3));
    a.digitalWrite(5,binary_small_audio_enveloped_out(i,4));
    pause(delay)
end
end

% Text input for downsampling.
function edit8_Callback(hObject, eventdata, handles)
% hObject    handle to edit8 (see GCBO)
% eventdata  reserved - to be defined in a future version of MATLAB
% handles    structure with handles and user data (see GUIDATA)

% Hints: get(hObject,'String') returns contents of edit8 as text
%        str2double(get(hObject,'String')) returns contents of edit8 as a
double
global downsample_input
downsample_input=str2double(get(hObject,'String'));
```

```
end

% --- Executes during object creation, after setting all properties.
function edit8_CreateFcn(hObject, eventdata, handles)
% hObject    handle to edit8 (see GCBO)
% eventdata  reserved - to be defined in a future version of MATLAB
% handles    empty - handles not created until after all CreateFcns called

% Hint: edit controls usually have a white background on Windows.
%       See ISPC and COMPUTER.
if ispc && isequal(get(hObject,'BackgroundColor'),
get(0,'defaultUicontrolBackgroundColor'))
    set(hObject,'BackgroundColor','white');
end
end

% % Pushbutton to downsample the data.
% % --- Executes on button press in pushbutton28.
% function pushbutton28_Callback(hObject, eventdata, handles)
% % hObject    handle to pushbutton28 (see GCBO)
% % eventdata  reserved - to be defined in a future version of MATLAB
% % handles    structure with handles and user data (see GUIDATA)
% global audio_enveloped_out small_audio_enveloped_out downsample_input
% small_audio_enveloped_out=downsample(audio_enveloped_out,downsample_input);
% end

function edit9_Callback(hObject, eventdata, handles)
    global audio_length
% hObject    handle to edit9 (see GCBO)
% eventdata  reserved - to be defined in a future version of MATLAB
% handles    structure with handles and user data (see GUIDATA)

% Hints: get(hObject,'String') returns contents of edit9 as text
%        str2double(get(hObject,'String')) returns contents of edit9 as a
double
audio_length=str2double(get(hObject,'String'));
end

% --- Executes during object creation, after setting all properties.
function edit9_CreateFcn(hObject, eventdata, handles)
% hObject    handle to edit9 (see GCBO)
% eventdata  reserved - to be defined in a future version of MATLAB
% handles    empty - handles not created until after all CreateFcns called
% Hint: edit controls usually have a white background on Windows.
%       See ISPC and COMPUTER.
if ispc && isequal(get(hObject,'BackgroundColor'),
get(0,'defaultUicontrolBackgroundColor'))
    set(hObject,'BackgroundColor','white');
end
end
```

APPENDIX A2

Copy of table comparing various properties of pyralin precursors, taken from [55]

Precursors	Kapton PMDA/DADE	PI 2556 BTDA/ODA/MPD	PI 2566 6-FDA/ODA	PI 2611 BPDA/PPD
Possible sheet/film thickness [μm]	7.5–125	0.5–1.5	1.3–2.2	5.0–10.0
Viscosity[Pa · s]	—	3.8	1.2–1.6	11.0–13.5
Water uptake [%]	4	2–3	1.5	0.5
Elongation [%]	25–50	15	12	25
Glass transition temperature [°C]	> 360	> 320	290	> 400
Decomposition temperature [°C]	—	550	530	620
Density at 25°C [g/cm^3]	1.42	1.45	1.06	1.07
Volume resistivity [Ω · cm]	10^{17}	$> 10^{16}$	—	$> 10^{16}$
Coefficient of thermal expansion CTE [$10^{-5} \cdot K^{-1}$]	2.0	4.0	6.0	0.3
Permittivity ε_r at 1 kHz and 50% rel. humidity	3.5	3.3	2.9	2.9
Dielectric strength [V/cm]	$1.1 \cdot 10^6$	$2 \cdot 10^6$	—	$2 \cdot 10^6$
Dissipation factor tan δ at 1 kHz	0.0025	0.002	0.002	0.002
Tensile strength [kg/mm^2]	110–165	13.5	8	35
Young's modulus [kg/mm^2]	255	245	175	845

BPDA: 3,3′, 4,4′-Biphenyl-Tetracarboxyl-Dianhydrid; BTDA: 3,3′, 4,4′-Benzophenon-Tetracarboxyl-Dianhydrid; DADE: 4,4′-Diamino-Diphenyl-Ether; FDA: Fluorinated Dianhydrid; ODA: Oxidiamine; PPD: p-Phenyl-Dianhydrid.

APPENDIX A3

Force Measurement Results of ITD+TFA Assemblies:

	ITD+TFA 1			ITD+TFA 2			ITD+TFA 3		
Distance	V	H	V/H	V	H	V/H	V	H	V/H
2 mm	0.77	0.37	2.08	0.89	0.36	2.47	0.71	0.41	1.73
4 mm	1.47	1.20	1.23	1.37	1.15	1.19	1.11	0.78	1.42
6 mm	1.89	1.55	1.22	1.62	1.32	1.23	1.27	1.02	1.25
8 mm	2.26	2.32	0.97	2.25	1.48	1.52	1.98	1.30	1.52
10 mm	2.53	2.45	1.03	2.65	1.51	1.75	2.35	1.58	1.49
Average	1.78	1.58	**1.31**	1.76	1.16	**1.63**	1.48	1.02	**1.48**

Force Measurement Results of IE+TFA Assemblies:

	IE+TFA 1			IE+TFA 2			IE+TFA 3		
Distance	V	H	V/H	V	H	V/H	V	H	V/H
2 mm	0.34	0.28	1.21	0.32	0.18	1.78	0.31	0.14	2.21
4 mm	0.48	0.26	1.85	0.30	0.16	1.88	0.66	0.29	2.28
6 mm	1.08	0.52	2.08	0.85	0.53	1.60	0.87	0.65	1.34
8 mm	1.48	0.81	1.83	0.93	0.59	1.58	1.34	0.72	1.86
10 mm	1.44	0.99	1.45	1.32	0.74	1.78	1.55	1.03	1.50
Average	0.96	0.57	**1.68**	0.74	0.44	**1.72**	0.95	0.57	**1.84**

Average Assembly Forces and Measured Component Forces:

	ITD			IE			ITD+TFA			IE+TFA		
Distance	V	H	V/H	V	H	V/H	V	H	V/H	V	H	V/H
2 mm	1.07	0.98	1.09	0.07	0.08	0.88	0.79	0.38	2.08	0.32	0.20	1.74
4 mm	1.23	0.92	1.34	0.07	0.07	1.00	1.32	1.04	1.28	0.48	0.24	2.00
6 mm	1.16	1.18	0.98	0.10	0.10	1.00	1.59	1.30	1.23	0.93	0.57	1.67
8 mm	1.19	1.08	1.10	0.11	0.12	0.92	2.16	1.70	1.34	1.25	0.71	1.75
10 mm	1.28	1.05	1.22	0.17	0.17	1.00	2.51	1.85	1.42	1.44	0.92	1.58
Avg (10mm)	1.19	1.04	**1.15**	0.10	0.11	**0.96**	1.67	1.25	**1.47**	0.88	0.53	**1.75**
Avg (6mm)	1.15	1.03	1.14	0.08	0.08	0.96	1.23	0.91	1.53	0.58	0.33	1.80
Avg % diff	*-0.03*	*-0.01*	*-0.01*	*-0.23*	*-0.23*	*0.00*	*-0.26*	*-0.28*	*0.04*	*-0.35*	*-0.36*	*0.03*

REFERENCES

[1] Pleis JR, Lethbridge-Cejku M. Summary health statistics for U.S. adults: National Health Interview Survey, 2006. National Center for Health Statistics. Vital Health Stat 10(235), 2007.

[2] "Cochlear Implants"*, National Institute on Deafness and Other Communication Disorders*, NIH Publication No. 11-4798, March 2011.

[3] B. Wilson and M. Dorman, "Cochlear implants: Current designs and future possibilities," *Journal of Rehabilitation Research and Development*, 45(5): 696-730, 2008.

[4] R. C. Bilger, F. O. Black, N. T. Hopkinson, E. N. Myers, J. L. Payne, N. R. Stenson, A. Vega, and R. V. Wolf, "Evaluation of subjects presently fitted with implanted auditory prostheses," *Ann. Otol. Rhinol. Laryngol.*, vol. 86, no. 3, pt. 2, pp. 1–176, 1977.

[5] Xu L, Pfingst BE. Spectral and temporal cues for speech recognition: implications for auditory prostheses. *Hear Res*. 2008;242:132-140.

[6] Bhatti PT, Lee S, Wise KD. A 32-site 4-channel cochlear electrode array. *IEEE J Solid-State Circuits*. 2006;41:2965-2973.

[7] Falcone JD. *Validation of High Density Electrode Arrays for Cochlear Implants: A Computational and Structural Approach* [thesis]. Atlanta: Georgia Institute of Technology; 2011.

[8] Iverson KC, Bhatti PT. Cochlear Implantation Using Thin Film Arrays, *Otolaryngology–Head and Neck Surgery*, vol. 144 no. 6 934-939, June 2011.

[9] Richmond DR. Yelverton JT, Fletcher ER. Phillips YY. Physical correlates of eardrum rupture. Ann Otol Rhinol Laryngol Suppl 1989:98(suppl 140):35-41.

[10] Gan RZ, Reeves BP. Wang X. Modeling of sound transmission from ear canal to cochlea. Ann Biomed Eng 2007;35:2180-2195.

[11] Principles of Neural Science, 4th Ed. Editors Eric R Kandel, James H Schwartz, Thomas M Jessell. McGraw-Hill, New York. 2000.

[12] Engineering Noise Control, 3rd Ed. Editors David A. Bies, Colin H. Hansen. Spon Press, New York. 2003. Pp. 69-76.

[13] Cochlear Function, General. James V Crawford, Michael J Ruckenstein. Emedicine.medscape.com

[14] An Introduction to the Physiology of Hearing, 3rd Ed. James O Pickles. Emerald Group Publishing Ltd, 2008.

[15] Murugasu and Russell, 1996.

[16] Robertson and Johnston, 1979.

[17] Roberto M, Hamernik RP, Turrentine GA. Damage of the auditory system associated with acute blast trauma. Ann Otol Rhinol Laryngol Suppl 1989;98(suppl l40):23-34.

[18] Rao DB. Moore DR. Reinke LA, Fechter LD. Free radical generation in the cochlea during combined exposure to noise and carbon monoxide: an electrophysioloizical and an EPR study. Hear Res 2001:161:113-22.

[19] Duan et al. *http://www.pnas.org/content/97/13/6939/F1.expansion.html.* Accessed 2/1/2012.

[20] Duan M, Qiu J. Dose and time-dependent protection of the antioxidant N-L-acetylcysteine against impulse noise trauma. Hearing Research 192(2004)1-9.

[21] National Institutes of Health, "Cochlear implants," *NIH Consensus Statement*, vol. 7, no. 2, pp. 1–9, 1988.

[22] National institutes of health, “Cochlear implants in adults and children”, *NIH Consensus Statement*, vol. 13, no. 2, pp. 1–30, 1995.
[23] Adapted from: “Cochlear Implants”. http://www.sgh.com.sg/clinical-departments centers/hearingandearimplant/services/pages/cochlear-implants.aspx, 02/02/2012.
[24] Loizou, PC. Mimicking the Human Ear: An Overview of Signal Processing Techniques for Converting Sound into Electrical Signals in Cochlear Implants. *IEEE Signal Processing Magazine*, 1998; pp. 101 – 130.
[25] Zrunek M., Lischka M. Dimensions of the Scala Tympani in Relation to the Diameters of Multichannel Electrodes, *Archives of Oto-Rhino-Laryngolog.*Spring-Verlag, 1980. pp. 159-165.
[26] Wilson B. Finley C. Lawson D. Better Speech Recognition with Cochlear Implants, *Nature*, vol. 352, pp. 236-238, July 1991.
[27] Boex C. Pelizzone M. Improvements in speech recognition with the CIS strategy for the Ineraid multichannel intracochlear implant, *Advances In Cochlear Implants* (Hochmair I. and Hochmair E., eds.), Vienna: Manz, 1994. pp. 136-140.
[28] Seligman P. McDermott H. Architecture of the Spectra 22 Speech Processor, *Annals of Otology, Rhinology, and Laryngology*, pp. 139-141, 1995.
[29] HiRes Fidelity 120® Sound Processing Technical Datasheet, Advanced Bionics, LLC, 2009.
[30] J. B. Firszt, D. B. Koch, M. Downing, and L. Litvak, “Current steering creates additional pitch percepts in adult cochlear implant recipients,” *Otology and Neurotology*, 28:629-636, 2007.
[31] K. Iverson, P. T. Bhatti, J. D. Falcone, R. Figueroa, and B. J. McKinnon, “Cochlear Implantation Using Thin-Film Array Electrodes,” *Otolaryngology-Head and Neck Surgery*, vol. 144, no. 6, pp. 934-939, Jun. 2011
[32] S. Rebscher, Department of Otolaryngology/Head and Neck Surgery, University of San Francisco, San Francisco, CA, Personal communication, 2011.
[33] Van Weert S, Stokroos R J. Effect of per-modiolar cochlear implant positioning on auditory nerve responses: A neural response telemetry study. *Acta Oto-Laryngologica*, 2005;725-731.
[34] Hagr A. Intra-Operative Neural Response Telemetry and Acoustic Reflex Assessment using an Advance-In-Stylet Technique and Modiolus-Hugging: A prospective cohort study. *Sultan Qaboos Univ Med J*. 2011 Aug;11(3):369-76.
[35] R Briggs, M Tykocinski. Development and evaluation of the modiolar research array – multi-centre collaborative study in human temporal bones. *Cochlear Implants International*, 2011 vol.12 no. 3; 129 – 139.
[36] S. Rebescher, A. Hetherington. Considerations for the design of future cochlear implant electrode arrays: Electrode array stiffness, size and depth of insertion. *Journal of Rehabil Res Dev*, 2008; 45(5): 731-748.
[37] Wardrop P, Whinney D, Rebscher SJ, Luxford W, Leake P. A temporal bone study of insertion trauma and intracochlear position of cochlear implant electrodes. Ii: Comparison of spiral clarion and hifocus ii electrodes. Hear Res 2005;203:68–79. [PubMed: 15855031].
[38] S. A. Shamma-Donoghue, G. A. May, “Thin-Film Multielectrode Arrays for a Cochlear Prosthesis,” *IEEE Transactions on Electronic Devices*, vol. ED-29, No. 1, January 1982; pp. 136-144.
[39] G.E. Loeb, R.A. Peck. Microminiature molding techniques for cochlear electrode arrays. *Journal of Neuroscience Methods 63*, 1995; 85-92.
[40] Brummer S, McHardy J, Turner MJ. "Electrical stimulation with Pt electrodes: Trace analysis for dissolved Pt and other dissolved electrochemical products," Brain Behav. Evol., vol. 14, p. 10, 1977.

[41] B. Wilson, M. Dorman. Cochlear Implants: Current designs and future possibilities. *Journal of Rehabilitation Research and Development, 2008; vol. 45, no. 5: 695-730*.
[42] Smith ZM, Delgutte B, Oxenham AJ. Chimeric Sounds reveal dichotomies in auditory perception. Nature, 2002; pp. 87-90.
[43] D. Lazard, P. Bordure. Speech perception performance for 100 post-lingually deaf adults fitted with Neurelec cochlear implants: comparison between Digisonic Convex and Digisonic SP devices after a 1-year follow-up. *Acta Oto-Laryngologica*, 2010; Early Online, 1–7.
[44] Neurelec Implant Brochure. http://www.neurelec.com/images/photos/Neurelec-Implant-engLow.pdf, 2/25/2012.
[45] Neurelec Saphyre Brochure. http://www.neurelec.com/images/photos/BroSAPHYR_EN.pdf, 2/25/2012.
[46] Coclear Product Launch Timeline. http://www.cochlear.com/files/assets/timeline.swf, 2/25/2012.
[47] MED-EL Announces U.S. Launch of New MAESTRO™ Cochlear Implant System. http://eon.businesswire.com/news/eon/20110913007576/en/Cochlear-Implant/MED-EL/MAESTRO-Cochlear-Implant-System , 2/25/2012.
[48] MED-EL OCncert – world's smallest and lightest titanium implant. http://www.medel.com/data/downloads/MAESTRO_US/Concert_Factsheet.pdf , 2/25/2012.
[49] HiResolution Bionic Ear System. http://www.advancedbionics.com/content/dam/ab/Global/en_ce/documents/libraries/Professional%20Library/AB%20Studies%20and%20Research/Research%20Highlights/AB_Research_Summaries_and_Publications_List.pdf , 2/25/2012.
[50] Cochlear Implant Technology Comparison Chart. http://www.advancedbionics.com/content/dam/ab/Global/en_ce/documents/candidate/AB_Cochlear_Implant_Technology_Comparison_Chart.pdf, 2/25/2012.
[51] HiRes 90K Implant. http://www.advancedbionics.com/us/en/products/hires_90k_implant.html , 2/25/2012.
[52] K. Najafi, K.D. Wise, "An Implantable Multielectrode Array with On-Chip Signal Processing," IEEE J. Solid-State Ckts., Vol. SC-21, No. 6, pp. 1035-1044, 12/1986.
[53] S. Myllymaa, K. Myllymaa, H. Korhonen. Fabrication and testing of polyimide-based microelectrode arrays for cortical mapping of evoked potentials. *Biosensors and Bioelectronics 24*, 2009: 3067–3072.
[54] Cheung, K.C., Renaud, P., Tanila, H., Djupsund, K. Flexible polyimide microelectrode array for in vivo recordings and current source density analysis. Biosensors amd Bioelectronics, 2007; 228:1783–1790.
[55] Stieglitz, T., Beutel, H., Schuettler, M., Meyer, J.-U. Micromachined, Polyimide-Based Devices for Flexible Neural Interfaces, *Biomedical Microdevices*, 2000; 283-294.
[56] N. Lago, K. Yoshida. Assessment of Biocompatibility of Chronically Implanted Polyimide and Platinum Intrafascicular Electrodes. *IEEE Transactions on Biomedical Engineering*, 2007; vol. 54 no. 2: 281-290.
[57] X. Xue, B. Pfingst. Inner Ear Implants for experimental electrical stimulation of auditory nerve arrays. *Journal of Neuroscience Methods,* 1989; vol 28: 189-196.
[58] J. Lotters et al. The mechanical properties of the rubber elastic polymer polydimethylsiloxane for sensor applications. *Journal of Micromechanics and Microengineering*, 1997; Vol. 7, No. 3: 145.
[59] PDMS Material Properties. http://www.mit.edu/~6.777/matprops/pdms.htm , 2/25/2012.
[60] NuSil MED-2000 Datasheet. http://www.nusil.com/library/products/MED-2000P.pdf , 2/25/2012.
[61] MED-EL FSP Clinical Trial, 2008. http://cochlearimplantonline.com/site/wp-content/uploads/2011/01/Cochlear-Implant-Brand-Comparison-latest-models-only.pdf

[62] Hereditary Hearing Loss Database. 2/2/2012 http://hereditaryhearingloss.org/main.aspx?c=.HHH&n=86597
[63] Y. S. Lim, S. Park, Y. Kim. Three-dimensional analysis of electrode behavior in a human cochlear model. *Medical Engineering and Physics*, 2005; vol. 27: 695-703.
[64] "Anatomy of the Human Ear", adapted from. http://en.wikipedia.org/wiki/File:Anatomy_of_the_Human_Ear.svg
[65] "Section through the spiral organ of Corti. Magnified. (G. Retzius)" & "Diagrammatic longitudinal section of the cochlea". *20th U.S. edition of Gray's Anatomy of the Human Body,* 1918.